Unusual roles of secretory SNARE SYP132 in plasma membrane H^+-ATPase traffic and vegetative plant growth

Author names and affiliations:

Lingfeng Xia[1], Maria Mar Marquès-Bueno[1,2], Craig Graham Bruce[1], Rucha Karnik[1,§]

[1] Plant Science Group, Laboratory of Plant Physiology and Biophysics, Institute of Molecular, Cell and Systems Biology, University of Glasgow, Glasgow G12 8QQ, United Kingdom

[2] Current address: Department of Molecular Genetics, Centre for Research in Agricultural Genomics (CRAG), CSIC-IRTA-UAB-UB, Campus UAB Bellaterra (Cerdanyola del Vallès), Barcelona, Spain

[§] Address correspondence to rucha.karnik@glasgow.ac.uk

Short title: SYP132 affects plasma membrane H^+-ATPase traffic

One-sentence summary: The secretory SNARE SYP132 affects auxin-regulated traffic of plasma membrane H^+-ATPase proteins and influences their roles in plant growth and homeostasis.

Author contributions: RK conceived research plans and designed the experiments; RK and LX prepared constructs; MMB, LX and RK did plant propagation and transgenic line preparation; RK and LX did the imaging experiments; MMB did RT-qPCR experiments; LX and RK did genotyping experiments, LX and RK did membrane partitioning experiments and immunoblots; LX did the yeast interaction assays; LX, MMB and RK did plant phenotype experiments; RK, LX and MMB analysed data. CB provided technical assistance for all experiments. RK wrote the manuscript with contributions from LX.

Funding:

This work was supported by the Royal Society University Research Fellowship UF150364 and Royal Society research grant RG160493 to RK. LX is funded by a PhD scholarship from the China Scholarship Council. CB and MMB were supported by the University of Glasgow Leadership funds to RK.

ABSTRACT

The plasma membrane proton (H^+)-ATPases of plants generate steep electrochemical gradients and activate osmotic solute uptake. H^+-ATPase-mediated proton pumping orchestrates cellular homeostasis and is a prerequisite for plastic cell expansion and plant growth. All evidence suggests that the population of H^+-ATPase proteins at the plasma membrane reflects a balance of their roles in exocytosis, endocytosis, and recycling. Auxin governs both traffic and activation of the plasma membrane H^+-ATPase proteins already present at the membrane. As in other eukaryotes, in plants, SNARE (soluble N-ethylmaleimide-sensitive factor attachment protein receptor)-mediated membrane traffic influences the density of several proteins at the plasma membrane. Even so, H^+-ATPase traffic, its relationship with SNAREs, and its regulation by auxin have remained enigmatic. Here, we identify the Arabidopsis (*Arabidopsis thaliana*) Qa-SNARE SYP132 (Syntaxin of Plants 132) as a key factor in H^+-ATPase traffic and demonstrate its association with endocytosis. SYP132 is a low abundant, secretory SNARE that primarily localizes to the plasma membrane. We find that *SYP132* expression is tightly regulated by auxin and that augmented SYP132 expression reduces the amount of H^+-ATPase proteins at the plasma membrane. The physiological consequences of SYP132 over-expression include reduced apoplast acidification and suppressed vegetative growth. Thus, SYP132 plays unexpected and vital roles in auxin-regulated H^+-ATPase traffic and associated functions at the plasma membrane.

INTRODUCTION

The P-type ATPase subfamily, plasma membrane proton (H^+)-ATPases are among the most important ion pumps in plants. They extrude protons against an electrochemical gradient with the expenditure of ATP to generate strong proton motive forces which energise H^+-coupled transport and ion flux at the plasma membrane (Palmgren, Sze et al., 1999, Sondergaard et al., 2004). These plasma membrane H^+-ATPases drive various processes including osmotic nutrient uptake and stomatal opening, they facilitate salt tolerance and regulate intracellular pH, and are essential for apoplast acidification and plastic cell wall loosening during vegetative growth (Sondergaard et al., 2004, Palmgren et al., 2011, Merlot et al., 2007).

Cell expansion is an essential process underlying plant growth and development. Growth begins with loosening of the rigid cell wall and an increase in turgor following osmotic water uptake. Secretory traffic delivers new membrane and wall materials for a growing cell (Cosgrove, 1987, Karnik et al., 2017, Hager, 2003). The long standing 'acid growth' hypothesis attributes cell wall loosening and osmotic cell expansion to the activity of H^+-ATPases. Thus, for plant growth and homeostasis, the plasma membrane H^+-ATPases must be tightly regulated (Hager et al., 1991, Rayle and Cleland, 1970, Hager et al., 1971).

The phytohormone auxin triggers 'acid growth' by activation of H^+ pumping, enhancing H^+-ATPase expression and affecting membrane traffic of the plasma membrane H^+-ATPases. Hager et al. (1991) noted a significant increase in membrane density of H^+-ATPases within few minutes of auxin treatment, attributed to membrane traffic, and demonstrated that a chemically induced block of protein synthesis diminished the auxin-enhanced density of H^+-ATPase proteins. In general, the density of membrane proteins is a balance between their forward traffic or exocytosis and their removal via endocytosis from the plasma membrane (Geldner et al., 2003). Therefore, different components of membrane traffic must accommodate the steady-state turnover as well as more rapid, auxin-induced increase in the density of H^+-ATPase proteins at the plasma membrane. Thus, while the 'acid-growth'

hypothesis remains an important framework for understanding role of auxin in cell expansion (Hager, 2003, Rayle and Cleland, 1970), it belies a simple interpretation in the context of post-translational modifications.

More than two decades have passed since the 'acid growth' hypothesis established the importance of both membrane traffic and the functional activation of the H^+-ATPases. Yet, we know very little about the mechanisms underlying H^+-ATPase membrane traffic or about its tissue- and isoform-specific regulation. In Arabidopsis, three Autoinhibited H^+-ATPase isoforms (AHA1, AHA2 and AHA11) are expressed throughout the plant (Arango et al., 2003, Harper et al., 1989, Palmgren, 2001). Amongst these, *AHA1* and *AHA2* together constitute almost 80% of H^+-ATPase mRNA transcripts and proteins (Haruta and Sussman, 2012). AHA1 and AHA2 show functional redundancy based on their T-DNA mutants (Haruta et al., 2010), even though recent studies suggest tissue specific functions of AHA1 in mediation of blue light responses and stomatal opening (Yamauchi et al., 2016).

Membrane proteins are usually synthesized in the endoplasmic reticulum and are trafficked through the Golgi from which they are sorted to the plasma membrane, tonoplast, or other target membranes. Alternate forward trafficking pathways also exist that bypass the Golgi in plants (Di Sansebastiano et al., 2017). In all eukaryotes, secretory traffic to the plasma membrane is mediated by SNARE proteins. They also drive the traffic of membrane proteins and soluble cargo between various endomembrane compartments and the plasma membrane. The different subfamilies of SNARE proteins are classified by the presence of universally conserved Qa-, Qb-, Qc-, and R-SNARE amino acid motifs. Qa-SNAREs, commonly referred to as Syntaxins are generally located on the target membrane while the R-SNAREs, also known as VAMPs (vesicle-associated membrane proteins) generally reside on the vesicle membrane (Jahn and Scheller, 2006). SNARE-mediated vesicle traffic occurs following assembly of the Qa- and R- SNAREs in a ternary SNARE complex with the Qb- and Qc-SNAREs, or the SNAP25-related (synaptosome-associated protein of 25 kDa) Qbc-

SNAREs, which draws the vesicle and target membranes in close proximity for fusion (Fasshauer et al., 1998, Bock et al., 2001).

In Arabidopsis, three Qa-SNAREs, SYP121 (Syntaxin of Plants 121, =SYR1/PEN1) and its close homologs SYP122 and SYP132, are ubiquitously expressed at the plasma membrane throughout plant development (Enami et al., 2009). SYP132 expression makes up a minor portion of the Qa-SNAREs at the plasma membrane. Thus, together, SYP121 and SYP122 drive a bulk of secretory traffic to the plasma membrane (Enami et al., 2009, Tyrrell et al., 2007, Karnik et al., 2015). Distinct, yet complementary pathways of SYP121- and SYP122-mediated secretory traffic affect vegetative plant growth (Waghmare et al., 2018, Karnik et al., 2015). Studies using dominant negative and mutant approaches showed that SYP121 and SYP122 do not affect plasma membrane H^+-ATPase traffic (Sutter et al., 2006, Geelen et al., 2002). Indeed, the SNARE regulatory protein, PATROL1, which is known to affect H^+-ATPase traffic, does not associate with SYP121 and SYP122 (Higaki et al., 2014). Thus, multiple lines of evidence discount any role of these two major Qa-SNAREs in H^+-ATPase traffic.

All the above observations leave unresolved the mechanism for H^+-ATPase traffic to and from the plasma membrane. Whether the plasma membrane H^+-ATPases are differentially regulated between plant tissues is also yet to be addressed. Using AHA1 as a model to study H^+-ATPase traffic together with the total H^+-ATPase population, here we report an unexpected role for Qa-SNARE SYP132 (Enami et al., 2009, Ichikawa et al., 2014) in the regulation of density of the H^+-ATPase proteins at the plasma membrane of root and shoot epidermal cells. Remarkably, we find that modulating SYP132 expression affects clathrin sensitive H^+-ATPase traffic from the plasma membrane, is subject to hormone auxin, and affects apoplastic acidification and plant growth. Thus, we suggest that SYP132 and associated endocytosis are vital for plasma membrane H^+-ATPase traffic and play a major role in the physiology of plant growth and morphogenesis.

RESULTS

The Qa-SNAREs SYP111, SYP121, SYP122, and SYP132 are all expressed throughout the plant and form cognate SNARE complexes with the Qbc-SNARE SNAP33 and the R-SNAREs VAMP721 and VAMP722 (El Kasmi et al., 2013, Enami et al., 2009, Ichikawa et al., 2014). Both SYP111 (or KNOLLE) and SYP132 mediate vesicle traffic at the phragmoplast to support cytokinesis (Enami et al., 2009, Sanderfoot, 2007, Park et al., 2018). Whilst SYP111 expression is cytokinesis specific, SYP132 occurs throughout plant development and likely has additional, yet undefined roles in traffic at the plasma membrane. SYP132 has been implicated in plant-microbe interactions, the secretion of defense-related peptides at the plasma membrane and in basic plant growth (Catalano et al., 2007, Kalde et al., 2007, Limpens et al., 2009, Pan et al., 2016, Huisman et al., 2016, Ichikawa et al., 2014, Enami et al., 2009). However, like the *aha1/aha2* double mutant, transfer DNA (T-DNA) insertional mutants of *syp132* are embryo lethal (Park et al., 2018).

SYP132 modulates AHA1 localization at the plasma membrane.

In the absence of a viable mutational strategy, we checked if SYP132 affects the cellular distribution of AHA1, by transiently co-expressing mCherry-AHA1 with green fluorescent protein (GFP)-fused SYP121 or SYP132 in *Nicotiana tabacum* leaf epidermis. This heterologous system has served as a useful model for initial studies involving Arabidopsis SNAREs and plasma membrane H^+-ATPases in the past (Foresti et al., 2006, Sutter et al., 2006, Karnik et al., 2013, Zhang et al., 2015). Samples were treated with water before imaging (Figure 1A). Additionally, for quantitative analysis, plasmolysis was induced (Supplemental Figure S1) as an aide to resolve cell interior and to visualise the distribution of the fluorophore-fused proteins following retraction of the plasma membrane from the cell wall (Rafiqi et al., 2010).

The mCherry-AHA1 and GFP-SYP132 protein distribution at the cell periphery relative to cell interior was determined by tracing around retracted cell periphery, region of interest (ROI) width ~1.5 um and the interior of each cell using the bright field overlay for reference. Integrated fluorescence density within the ROIs marking the periphery and interior of each cell was measured and corrected total fluorescence for each ROI was calculated following background subtraction (Marwaha and Sharma 2017). When co-expressed with GFP-SYP132, periphery/internal corrected total fluorescence ratio for mCherry-AHA1 was lower compared to when mCherry-AHA1 was expressed on its own or with GFP-SYP121 (Figure 1D). These data show that co-expression of GFP-SYP132 leads to an increase in the proportion of mCherry-AHA1 present inside the cells, while the proportion of mCherry-AHA1 at the cell periphery is reduced.

SYP132 affects AHA1 internalization from the plasma membrane.

To determine the effect of blocking SYP132 function on H^+-ATPase density, a dominant negative fragment strategy was employed. In this case, we used a soluble fragment of the Qa-SNARE, the SYP132$^{Habc\Delta}$ which lacks the conserved H3 domain containing the Qa-SNARE motif as well as the transmembrane domain (Supplemental Figure S2A-E). Together, both domains of the Qa-SNARE are necessary for vesicle fusion and secretory traffic at the plasma membrane (Sutter et al., 2006, Karnik et al., 2013, Geelen et al., 2002). The Qa-SNARE$^{Habc\Delta}$ or the so-called Sp3-fragments retain the interactive surfaces associated with cognate partner binding, however they lose interactions with high molecular weight regulatory proteins and ion transporters (Kargul et al., 2001). We used the yeast GPI signal peptide-anchored split-ubiquitin (GPS) system, which allows detection of soluble bait protein binding (Zhang et al., 2018), to test interactions of the SYP132$^{Habc\Delta}$. We observed that SYP132$^{Habc\Delta}$ retains one-to-one binding with the cognate SNAREs SNAP33 or VAMP721 and with the full length SYP132 (Supplemental Figure S2). These interactions of SYP132$^{Habc\Delta}$ were similar to those of SYP132$^{\Delta C}$ (Supplemental Figure S2), the conventional

dominant negative or the so-called Sp2 fragment, which lacks C-terminal transmembrane domain (Karnik et al., 2015, Grefen et al., 2015, Karnik et al., 2013, Karnik et al., 2017, Sutter et al., 2006).

Additionally, the dominant negative effect of SYP132$^{Habc\Delta}$ in blocking secretory traffic at the plasma membrane was verified by assaying the traffic of cargoes that are known to be secreted. This technique (Waghmare et al., 2018) yields increased intracellular fluorescence if a fluorophore-fused secretory cargo accumulates within the secretory pathway due to the block of its traffic. The accumulation is quantified relative to the fluorescence of a non-secretory marker that is expressed at the same time. The cargoes were each fused with mCherry and co-expressed with the GFP protein fused with an ER-retention HDEL motif (GFP-HDEL) using a tricistronic vector (Supplemental Figure S3A) that ensures equal genetic loads on transformation. GFP-HDEL is retained in the ER and serves as a marker for transformation and for ratiometric fluorescence analysis of block of secretion in the assay (Waghmare et al., 2018, Karnik et al., 2013). The CO_2 Response Secreted Protease (SBT5.2) is a SYP132-dependent cargo and is secreted independent of the SYP121 and SYP122 nexus (Waghmare et al., 2018). In presence of SYP132 wild type, the mCherry/GFP ratio for mCherry-SBT5.2 was considerably lower compared to that of the non-secreted mCherry (control) indicating secretion of this cargo. However, in presence of SYP132$^{Habc\Delta}$, the mCherry/GFP ratio for mCherry-SBT5.2 was comparable to the non-secreted control (Supplemental Figure S3B). These data showed that secretion of the mCherry-SBT5.2 is reduced in presence of SYP132$^{Habc\Delta}$. The secretion of SYP132-independent cargo mCherry-Meristem 5 (MERI-5) (Waghmare et al., 2018) was not affected by SYP132 wild type and only a marginal effect was observed in presence of SYP132$^{Habc\Delta}$ (Supplemental Figure S3), plausibly a consequence of titrating the cognate SNAREs that are shared between SYP121, SYP122 and SYP132. Thus, the SYP132$^{Habc\Delta}$ acts as dominant negative and its over-expression blocks SYP132-dependent secretory traffic to the plasma membrane.

We anticipated that inducing constitutive over-expression of SYP132$^{Habc\Delta}$ would interfere with SYP132-mediated secretory traffic to the plasma membrane with specificity (Tyrrell et al., 2007). Surprisingly, however, following over-expression of the dominant-negative GFP-SYP132$^{Habc\Delta}$, the cell periphery/internal fluorescence ratio for mCherry-AHA1 increased compared to mCherry-AHA1 expressed on its own or with GFP-SYP132 or GFP-SYP121 (Figure 1D). These data showed that mCherry-AHA1 localization to the cell periphery is augmented in the presence of the dominant negative GFP-SYP132$^{Habc\Delta}$.

As controls, each of the full-length Qa-SNAREs were expressed in Tobacco (*Nicotiana tabacum*) leaf epidermis. Confocal images showed that when expressed on their own, both SYP121 and SYP132 proteins are predominantly localized at the cell periphery (Figure 1B, Supplemental Figure S4). As anticipated for a soluble Qa-SNARE fragment, SYP132$^{Habc\Delta}$ the periphery/internal fluorescence ratio for RFP-SYP132$^{Habc\Delta}$ was significantly lower compared to the RFP-SYP132 (Figure 1B, Supplemental Figure S4) suggesting that the SYP132$^{Habc\Delta}$ fragment is localized to the cell interior.

Notably, compared to the SYP132 expressed on its own, the periphery/internal fluorescence ratio for GFP-SYP132 was lower when the Qa-SNARE was co-expressed with mCherry-AHA1. However, the cellular distribution of SYP121 was not affected by AHA1 co-expression (Figure 1 A-C, Supplemental Figure S4).

To test the specificity of SYP132 action, the Qa-SNARE was co-expressed with the K^+ channel KAT1. KAT1 delivery to the plasma membrane is affected in the *syp121* mutant plants (Eisenach et al., 2012) and mobility of the channel proteins within the plasma membrane is altered in the presence of the dominant negative fragment of SYP121 (Sutter et al 2006, 2007). Confocal images of Tobacco epidermal cells and their analysis showed that GFP-SYP132 has no effect on the distribution of mCherry-KAT1 puncta at the cell periphery or on their mobility. As expected, GFP-SYP121 altered mCherry-KAT1 distribution at the cell periphery (Supplemental Figure S5). These data suggest that the SNARE SYP132 has distinct roles associated with AHA1 traffic within the cell.

To confirm if SYP132 affects H^+-ATPase integration at the plasma membrane in different cell types, three-day-old Arabidopsis seedlings stably expressing 35S:GFP-AHA1 (Hashimoto-Sugimoto et al., 2013) were transiently transformed with red fluorescent protein (RFP) fused SYP121, SYP132 and SYP132$^{Habc\Delta}$. Root hair are single cells that are easy to isolate visually with a clear demarcation of cell interior, the plasma membrane, and outside of the cell. Therefore, confocal images of root hair were acquired following labelling of the plasma membrane with lipophilic FM4-64 dye on ice (Figure 2A). As a measure of integration of GFP-AHA1 into the plasma membrane, line scans across the plasma membrane were analysed (Figure 2B-C) to determine the overlap of GFP-AHA1 with FM4-64 fluorescence signals as a percentage of the total FM4-64 signal across each line scan. A higher percent total overlap with FM4-64 fluorescence in such analysis is therefore indicative of greater localization to the plasma membrane (Sklodowski et al., 2017). GFP-AHA1 expressed on its own (control) showed 85±3% fluorescence overlap with FM4-64, akin to co-expression with RFP-SYP121. However, when co-expressed with RFP-SYP132, the overlap of GFP-AHA1 with FM4-64 was significantly lower and conversely, co-expression with the RFP-SYP132$^{Habc\Delta}$ increased GFP-AHA1 overlap with FM4-64 (Figure 2C). Thus, abrogation of SYP132 function using the dominant negative SYP132$^{Habc\Delta}$ enhanced GFP-AHA1 localization at the plasma membrane.

It is notable that in transiently transformed cells, fluorophore-fused AHA1 appeared to localize in punctate structures in the interior of cells co-expressing SYP132 (Figures 1-3, Supplemental Figure S1). Similarly, GFP-AHA1 appeared in punctate structures within the interior of stomatal guard cells (Supplemental Figure S6 A, C) and root hairs (Supplemental Figure S6 B-C) in Arabidopsis stable lines co-expressing RFP-SYP132 under the constitutive 35S promoter (Supplemental Figure S6C). Together, these data demonstrate that SYP132 affects AHA1 localization within the cell in different tissue types and in both transient and stable systems.

SYP132-associated H^+-ATPase traffic is sensitive to clathrin-mediated endocytosis.

Previous studies had noted that plasma membrane H^+-ATPases accumulate in endosomal structures in some circumstances (Kitakura et al., 2011). Such H^+-ATPase traffic within the cells has been attributed to be clathrin-mediated endocytosis from the plasma membrane (Dhonukshe et al., 2007). To test if SYP132 causes AHA1 re-distribution to intracellular compartments (Figure 2A), possibly as a result of clathrin mediated endocytic traffic, we used the clathrin heavy chain 1 mutant, *chc1,* and stable Arabidopsis lines of the tamoxifen-inducible dominant negative mutant HUB1, which are deficient in clathrin-mediated endocytosis (CME) (Kitakura et al., 2011, Larson et al., 2017). Three-day-old wild type and clathrin mutant Arabidopsis seedlings were transiently transformed to express mCherry-AHA1 on its own and together with GFP-SYP132. In parallel experiments, seedlings from the same lines were labelled with FM4-64 and analyzed for internalization to ensure that block of CME was observed in the transgenic lines compared to the wild type seedlings (Gaffield and Betz, 2006). As a measure of internalization, mCherry-AHA1, GFP-SYP132, or FM4-64 distribution at cell periphery and interior was analyzed in the root hair cells. An outline was drawn around the cell interior and along the cell periphery and mean fluorescence was measured (Figure 3A). Ratio of internal/ periphery fluorescence following subtraction of background fluorescence (see Methods) was calculated and mean fluorescence ratios were plotted (Figure 3 B, D, F). In the *chc1* and HUB1 seedlings, FM4-64 uptake into the cell interior was reduced compared to that in wild type seedlings, thus confirming the block of CME (Figure 3A-B). In parallel experiments, when expressed on its own, mCherry-AHA1 showed marginal internalization in wild type root hair and in the clathrin mutant seedlings (Figure 3C-D). However, in seedlings where mCherry-AHA1 was co-expressed with GFP-SYP132, internal/periphery fluorescence ratio was considerably higher for both mCherry-AHA1 and GFP-SYP132 in the wild type Arabidopsis root hair, but not in the clathrin mutant lines (Figure 3E-F). Together, these data suggest that SYP132-associated re-distribution of

289 the H^+-ATPase proteins from the plasma membrane to intracellular compartments is
290 sensitive to clathrin.

SYP132 affects H^+-ATPase re-distribution from the plasma membrane.

mCherry-AHA1 internalization was observed only after co-expression of GFP-SYP132 (Figure 3, Supplemental Figure S6), although native SYP132 was present. In each of these experiments, GFP-SYP132 was constitutively over-expressed under the *Cauliflower* mosaic virus (*Ca*MV) 35S promoter. Therefore, we asked if H^+-ATPase traffic was linked to the levels of SYP132 expression. To augment SYP132 expression, wild type Arabidopsis were stably transformed (SYP132-OX) to constitutively over-express GFP- or RFP- fused SYP132 proteins. Two independent SYP132-OX lines which showed similar levels of fluorophore fused-SYP132 protein expression in the T3 generation (Supplemental Figure S7A) were chosen for experiments. Driven by the *Ca*MV 35S promoter, the SYP132-OX lines showed roughly a 13-fold higher expression while in the heterozygous *syp132* mutant (*syp132*^{T}) (Park et al., 2018) (Supplemental Figure S7B) expression was reduced by 5-fold lower when compared to the wild type plants (Supplemental Figure S7C).

To measure intracellular distribution of the H^+-ATPase proteins in each of these lines, Arabidopsis leaf microsomes were isolated and used to separate plasma membrane (PM) and internal membrane (IM) fractions, utilizing the aqueous two-polymer phase system (Sutter et al., 2007, Yoshida et al., 1983). Proteins in the PM and IM fractions were resolved by SDS-PAGE followed by immunoblot analysis. Purity of the enriched fractions was determined to be ~95% by immunoblot analysis using antibodies against KAT1 K^+-channel as a marker for the plasma membrane fraction and against the ER-resident lumenal-binding protein BiP as a marker for the total internal membrane fraction. Immunoblot analysis was carried out using anti-RFP (or anti-GFP) to detect the RFP (or GFP) fused SYP132 to detect distribution of this SNAREs in the PM and IM fractions. Immunoblot analysis using native Arabidopsis anti-H^+-ATPase antibodies which bind all isoforms of the AHAs (Figure 4A) detected total H^+-ATPase protein population in the membrane fractions. Immunoblot band intensities were analyzed by densitometry and normalized to total protein for each gel lane. Quantity of H^+-ATPase proteins, relative to wild type leaves was thus calculated and plotted

318 (Figure 4B-D). We found that the density of the H^+-ATPase proteins at the plasma
319 membrane when compared to the wild type leaves was two-fold higher in *syp132*^{T} leaves
320 while it was two-fold lower in the SYP132-OX leaves. In SYP132-OX leaves, majority of the
321 H^+-ATPase proteins were localized to the internal membranes (Figure 4 A-B). Total H^+-
322 ATPase protein density in microsomes was higher in the *syp132*^{T} leaves but there was no
323 obvious difference in total H^+-ATPase protein density between wild type and SYP132-OX
324 leaves (Figure 4C). A significant proportion of the RFP-SYP132 proteins were also localized
325 to the internal membranes (Figure 4D). Together these data suggest that SYP132 affects
326 total H^+-ATPase protein distribution to the plasma membrane.

327

328 **Modulation of SYP132 expression affects 'acid growth'.**

329 Given that SYP132 affected H^+-ATPase protein density at the plasma membrane, we
330 examined whether changes in this density translated to net H^+-ATPase activity at the plasma
331 membrane. As a measure of H^+ extrusion, the mean pH of the apoplast was measured by
332 water infiltration and centrifugation. Rosette leaves of three-week-old wild type, *syp132*^{T} and
333 SYP132-OX plants were infiltrated, immediately cut into strips, placed in spin columns, and
334 centrifuged to elute the apoplastic wash fluid (Grefen et al., 2015). The pH of the apoplast
335 wash fluid was measured using a calibrated micro pH electrode. Compared to the wild type
336 leaves, the mean apoplast wash fluid pH in SYP132-OX leaves was more alkaline while in
337 the *syp132*^{T} leaves, the pH was more acidic (Figure 5A). Thus, modulation of SYP132
338 expression affected H^+-ATPase density and net H^+ extrusion at the plasma membrane.

339 To test whether changes in H^+-ATPase density and net function affected plant growth, plant
340 growth was measured as a function of rosette area, shoot fresh weight (Hashimoto-
341 Sugimoto et al., 2013), and hypocotyl length. The various plant lines were cultivated under a
342 standard growth conditions for three weeks before growth above ground was assayed for
343 shoot weight and rosette area. In addition, hypocotyl length was measured from seedlings
344 following four days of growth in the dark. We found that the SYP132-OX plants exhibited a

345 reduced above-ground shoot growth on soil compared to the wild type and *syp132*^{T} plants
346 (Figure 5 B-G). These experiments were repeated in four independently transformed
347 transgenic SYP132-OX lines and each exhibited similar phenotype (Supplemental Figure
348 S8). As controls for this experiment, the SYP121-OX seedlings showed no significant
349 differences in shoot growth compared to the wild type seedling while as expected, the AHA1-
350 OX shoots which have increased population of the H^{+}-ATPase proteins at the plasma
351 membrane, grew bigger (Wang et al., 2014) (Supplemental Figure S9). Hypocotyl length in
352 dark grown SYP132-OX seedlings was shorter than in wild type seedlings but longer in
353 *syp132*^{T} seedlings (Figure 6H, Supplemental Figure S8D). Together, these data imply that
354 changes in H^{+}-ATPase protein density has direct implications on its function at the plasma
355 membrane; an increase in density of the H^{+}-ATPase proteins at the plasma membrane
356 promotes plant growth.

357

358 **Auxin regulates expression of the low abundant *Arabidopsis* Qa-SNARE SYP132.**

359 The phytohormone auxin regulates both activity and the density of H^{+}-ATPase proteins at
360 the plasma membrane (Hager, 2003, Hager et al., 1971) and its action one of the key tenets
361 of the acid growth hypothesis. Since SYP132 over-expression negatively regulates H^{+}-
362 ATPase protein density and function, we set out to determine if auxin has a role in
363 modulation of *SYP132* expression.

364 Auxin promotes growth in both shoot and root tissues at low concentrations (10^{-11} M), but at
365 higher concentrations of auxin (10^{-6} M) a temporal inhibition of primary root growth is
366 observed, noticeably within 45 to 180 minutes of treatment (Velasquez et al., 2016, Evans et
367 al., 1994). In shoots, auxin induces growth even at high concentrations (≥10^{-5} M) (Fendrych
368 et al., 2016). Thus, 10^{-6} M NAA has opposite effects on growth between root and shoot
369 tissue. We exploited this auxin-concentration dependence of plant growth to test if the
370 hormone regulates SYP132 expression differentially between root and shoot for the
371 promotion or suppression of plant growth.

To quantify root and shoot specific expression of *SYP132* transcripts in whole plant or separated roots and shoots, reverse transcription quantitative PCR (RT-qPCR) was carried out (Omelyanchuk et al., 2017). As a control subset, the transcript levels of *SYP121* and the root specific *SYP123* were assessed (Ichikawa et al., 2014, Bassham and Blatt, 2008). Figure 6A shows the transcript levels for each of these Qa-SNAREs in whole plants. Supplemental Table S4 lists RT-qPCR primer binding efficiencies, enabling transcript levels of the different SNAREs to be compared. These data confirmed that *SYP121* transcripts are higher by about 100-fold than *SYP123* and *SYP132* (Enami et al., 2009).

To determine the effect of auxin on Qa-SNARE expression, Arabidopsis seedlings were grown for 5-7 days on soft agar. The shoots were separated from roots at the hypocotyl junction prior to treatment with 10^{-6} M NAA for 60 and 180 minutes. No significant effects of auxin on expression of *SYP121* and *SYP123* transcripts were observed, however substantial differences were noted in the transcription of SYP132. Following auxin treatment, SYP132 transcripts decreased two-fold in shoots (Figure 6B), while they increased three-fold in roots (Figure 6C) compared to control. Thus, in high concentrations of auxin that promote growth, SYP132 transcript levels are concurrently down-regulated in shoots. Conversely, for the same concentrations of auxin that suppress growth in roots, SYP132 transcript abundance is up-regulated. In other words, the transcription of SYP132 parallels the actions of auxin on growth between the root and shoot.

Modulation of SYP132 expression affects stomatal apertures.

Stomatal opening depends on turgidity of the two stomatal guard cells; turgid guard cells hold open the stomatal pore and flaccid guard cells cause stomatal closure. Activation and membrane traffic of key transporters, including the H^+-ATPases in the guard cell plasma membrane is a major determinant of stomatal aperture regulation and its interaction with the environment (Hashimoto-Sugimoto et al., 2013, Yamauchi et al., 2016, Kinoshita and

Shimazaki, 1999, Eisenach et al., 2012, Jezek and Blatt, 2017, Vialet-Chabrand et al., 2017).

To test if modulation of SYP132 and its impact on H^+-ATPase traffic affects stomatal aperture, intact leaf stomatal apertures were measured in four-week-old plants grown in 150 µmol $m^{-2}s^{-1}$ PAR light (Chitrakar and Melotto, 2010) to compare the effects of SYP132 expression. We found that apertures in *syp132*^{T} plants were larger and conversely, that apertures of SYP132-OX plants were smaller compared to wild type (Figure 7).

As a primary transporter in stomatal guard cells, H^+-ATPase activation occurs following post-translational modifications of its C-terminus. Phosphorylation of the C-terminal regulatory domain of the H^+-ATPases, facilitates binding of 14-3-3 proteins and the release of autoinhibition (Palmgren, 2001). The fungal phytotoxin fusicoccin (FC) induces irreversible stomatal opening by stabilizing 14-3-3 protein binding and activation of the H^+-ATPases (Fuglsang et al., 2003, Marre, 1979). Thus, we also compared apertures following treatments with fusicoccin. We found that the fungal toxin increased stomatal opening in all the plant lines including the SYP132-OX (Figure 7). Together these data indicated that SYP132 negatively regulates stomatal aperture and this effect of SYP132 can be rescued by treatment with fusicoccin.

Hormones and fungal toxin fusicoccin affect SYP132-associated H^+-ATPase traffic.

The effects of fusicoccin treatment reflected in stomatal aperture measurements might be explained by enhanced activation of the H^+-ATPases present at the plasma membrane in the SYP132-OX lines. For example, if 14-3-3 binding blocks SYP132-associated H^+-ATPase traffic, it might thereby increase both the density and activity at the H^+-ATPases at plasma membrane. Alternatively, fusicoccin might augment H^+-ATPase expression and lead to a proportionate increase in density and function of the pumps at the plasma membrane. To distinguish between these different possibilities, we carried out fractionation of microsomes prepared from leaves treated with control (0.02% [v/v] ethanol in water), 10^{-6} M NAA (auxin)

and 10^{-5} M fusicoccin for two hours (Hashimoto-Sugimoto et al., 2013). Auxin treatment in these experiments served as an experimental control for its effects on enhancing H^+-ATPase activity at the plasma membrane. H^+-ATPase and RFP-SYP132 population in the plasma membrane (PM) and internal membrane (IM) fractions was estimated as a measure of density of respective bands in immunoblots and normalized to the total protein for each gel lane. These H^+-ATPase and RFP-SYP132 protein quantities were plotted relative to the wild type, control treatment samples (Figure 8A, Supplemental Figure S10).

We found that NAA treatment led to significant increases the H^+-ATPase protein density in plasma membrane. The plasma membrane to internal membrane ratio of H^+-ATPase protein was higher in wild type plants treated with NAA compared to control (Figure 8D). Indeed, Hager et al. (1991) had noted an increase in plasma membrane density of the H^+-ATPases following auxin treatment in maize coleoptiles. In the SYP132-OX leaves, NAA did not have any obvious effects on the distribution of the H^+-ATPases between the plasma membrane and endosomal compartments (Figure 8 A, B, D).

Following fusicoccin treatment, H^+-ATPase protein density increased in purified plasma membrane fractions from leaves of both wild type and SYP132-OX plants compared to the control (Figure 8 A, B, D, F). Total H^+-ATPase protein levels also showed a significant increase in wild type and SYP132-OX leaves following fusicoccin treatment compared to control (Figure 8F). In the SYP132-OX leaves, the plasma membrane to internal membrane fraction ratio of the H^+-ATPase proteins increased in fusicoccin treated leaves compared to control although the total H^+-ATPase protein density was lower than the wild type leaves. Thus, fusicoccin promoted an increase in H^+-ATPase protein density at the plasma membrane compared to the internal compartments, thereby reversing the effect of SYP132-OX. Corresponding to H^+-ATPase proteins, plasma membrane density of RFP-SYP132 also increased in fusicoccin treated leaves compared to control and NAA (Figure 8C). Therefore, we conclude that fusicoccin increases both total cellular and plasma membrane H^+-ATPase protein populations in wild type and SYP132-OX plants.

To test how plasma membrane H^+-ATPase protein distribution at the plasma membrane is regulated by a hormone that suppress its function, we carried out similar fractionation analyses after treating leaves with the plant stress hormone abscisic acid (ABA) for two hours. ABA is a negative regulator of H^+-ATPase phosphorylation and activity (Haruta et al., 2015) and it triggers stomatal closure (Thiel et al., 1993, Jezek and Blatt, 2017, Merlot et al., 2007, Xue et al., 2018).

Total cellular H^+-ATPase density was considerably reduced in both wild type and SYP132-OX leaves following ABA treatment. In wild type leaves, ABA treatment reduced the H^+-ATPase population in both plasma membrane and in internal membranes, compared to the control. In the SYP132-OX leaves, ABA treatment increased the plasma membrane to internal membrane ratio for H^+-ATPase proteins compared to the control (Figure 8 B, D, F). These data indicated that ABA in wild type plants promotes H^+-ATPase traffic to reduce H^+-ATPase density in both plasma and internal membranes. In SYP132-OX plants, where the population of the H^+-ATPase proteins at the plasma membrane is already reduced, ABA drives reduction of the H^+-ATPases in internal membranes.

In SYP132-OX leaves, following ABA treatment, the plasma membrane to internal membrane ratio for RFP-SYP132 was higher while the plasma membrane density of the fluorophore fused SNARE was reduced when compared to control, NAA, and fusicoccin treatments (Figure 8 C, E, G). These results suggested that ABA treatment reduces both plasma and internal membrane density of the RFP-SYP132.

Taken together, these data (Figure 8, Supplemental Figure S10) demonstrate that the hormones auxin and ABA affect the distribution of the H^+-ATPase proteins at the plasma membrane. Likely, H^+-ATPase traffic, in association with the SYP132, dictates the availability of the H^+-ATPase proteins at the plasma membrane for active function. A schematic model that consolidates our findings is shown in Figure 9.

DISCUSSION:

The Qa-SNAREs SYP121 and SYP122 are most abundantly expressed throughout the plant and mediate bulk transport and secretion of cargo at the plasma membrane (Karnik et al., 2017, Waghmare et al., 2018, Enami et al., 2009). By contrast, the plasma membrane Qa-SNARE SYP132 is expressed in low abundance throughout the plant (Ichikawa et al., 2014). Nevertheless, SYP121 and SYP122 are not vital to the survival of plants. This is evident from the *syp121/syp122* double mutants which are severely stunted in growth, and yet are able to complete the growth cycle and produce seeds (Assaad et al., 2004). However, SYP132 is essential for plant viability and the *syp132* mutant is embryo lethal (Park et al., 2018, Enami et al., 2009, Ichikawa et al., 2014). The studies outlined here identify SYP132 as a key player in H^+-ATPase traffic at the plasma membrane that is moderated by plant hormones such as auxin. Along with our other observations of H^+-ATPase function, this work demonstrates an unexpected role for SYP132 in functional regulation of proton transport. Two key lines of evidence support these findings. (1) SYP132 expression is inversely related to H^+-ATPase density at the plasma membrane, and (2) SYP132 expression is tissue-specific and consistently affects plasma membrane H^+-ATPase density and H^+ extrusion to the apoplast as well as stomatal apertures and vegetative growth. Most importantly, our study identifies that plant growth hormone auxin regulates *SYP132* expression; auxin-driven suppression of *SYP132* in growing shoots correlated with 'auxin-induced' increase in plasma membrane H^+-ATPase density and function. While we have focused in part on AHA1 as a model H^+-ATPase, we find that SYP132 affects H^+-ATPase localization in each of the tissue types examined. Our findings thus suggest that the SYP132 plays a critical role in promoting H^+-ATPase internalization from the plasma membrane in both roots and shoots and is an important part of the mechanics of auxin-mediated control of pump activity at the plasma membrane.

H^+-ATPase traffic at the plasma membrane unveiled by SYP132 dominant negative

Qa-SNAREs proteins are constituted of structural domains that are highly conserved across all eukaryotes and include a C-terminal transmembrane membrane anchor, a highly conserved H3-helix containing the SNARE motif vital for assembly of the SNARE core-complex, and regulatory Habc and N-terminal domains that fold back on the H3-helix to regulate cognate SNARE binding (Jahn and Scheller, 2006, Bassham and Blatt, 2008). All the domains of Qa-SNAREs contribute to the interactions essential for successful vesicle fusion events at the plasma membrane.

Dominant negative strategies involving the over-expression of the Qa-SNARE fragments lacking one or more of these domains have been employed successfully over the past decades to disrupt SNARE function and to study Qa-SNARE mediated secretory traffic (Kargul et al., 2001, Tyrrell et al., 2007, Sutter et al., 2006, Karnik et al., 2013, Grefen et al., 2015). Examples include the so-called Sp3-fragments $SYP121^{Habc\Delta}$, lacking the Qa-SNARE and C-terminal transmembrane domains essential for SNARE interactions (Kargul et al., 2001) and the so-called Sp2-fragments $SYP121^{\Delta C}$ and $SYP122^{\Delta C}$ lacking the C-terminal transmembrane domain required for targeted vesicle fusion at the plasma membrane (Tyrrell et al., 2007, Sutter et al., 2006). In this context it is worth noting that Sutter et al. (2006) used over-expression of the SYP121 Sp2-fragment and observed a block of KAT1 K^+ channel traffic to the plasma membrane. The SYP121 Sp2-fragment blocks traffic mediated by both SYP121 and SYP122 (Tyrrell et al., 2007). They used the plasma membrane H^+-ATPase as a control in these studies and reported that its cellular distribution was not affected by the SYP121 Sp2-fragment (Sutter et al., 2006). Thus, both SYP121 and SYP122 may be discounted for roles in H^+-ATPase traffic at the plasma membrane.

A major drawback of the dominant negative Sp2-fragment approach is the overlaps in block of the traffic mediated by other Qa-SNAREs which share common cognate SNARE binding partners in a SNARE complex for secretion. When over-expressed, the Sp2-fragments are able to form SNARE complexes but these complexes are not targeted to the plasma

membrane for vesicle fusion, resulting in a block of secretory vesicle traffic at the plasma membrane (Karnik et al., 2013, Karnik et al., 2017, Karnik et al., 2015, Tyrrell et al., 2007). Although all three Qa-SNAREs SYP121, SYP122, and SYP132 bind to the same cognate SNARE partners (Ichikawa et al., 2014, Karnik et al., 2013), they mediate vesicle traffic of distinct cargoes (Waghmare et al., 2018, Kalde et al., 2007). Therefore, the use of dominant negative strategies that confer specificity in action are desirable. We discovered that the SYP132 SP3 fragment, SYP132$^{Habc\Delta}$ blocked secretion of SYP132-dependent secretory cargo, but its effect on the traffic of cargos that rely on SYP132-independent pathways was much reduced (Supplemental Figure S3). This specificity of SYP132$^{Habc\Delta}$ can be attributed to the soluble SYP132$^{Habc\Delta}$ peptides (Supplemental Figure S4) that interact with the full-length SYP132 to inhibit its activity (Supplemental Figure S2F). Additionally, the Qa-SNARE N-terminus and Habc domains generally bind with regulatory proteins such as the SM (Sec1/Munc18- like) proteins (Sudhof and Rothman, 2009, Karnik et al., 2013, Karnik et al., 2015) which specifically regulate the Qa-SNARE function. For example, in Arabidopsis vegetative tissue, the SM protein SEC11 binds specifically with SYP121 to promote secretory traffic at the plasma membrane (Karnik et al., 2013), while the SM protein Sec1B is essential for SYP132-meditated secretory traffic to the plasma membrane (Karnahl et al., 2018). Hence, another possible explanation for SYP132$^{Habc\Delta}$ dominant negative action is that it may bind and titrate out the regulatory SM proteins essential for stabilized SNARE complex formation (Karnik et al., 2013), thereby suppressing SYP132-mediated secretory traffic at the plasma membrane.

In this study, the SYP132$^{Habc\Delta}$ fragment (Supplemental Figure S2A-E) was specifically used to block SYP132-mediated secretory traffic of the H^+-ATPases to the plasma membrane (Figure 1, 2). Logically, if SYP132 is involved in H^+-ATPase forward traffic, a block of SYP132-mediated secretion by the dominant negative SYP132$^{Habc\Delta}$ should perturb the delivery of the H^+-ATPases to the plasma membrane. Contrary to this supposition, SYP132$^{Habc\Delta}$ over-expression enhanced H^+-ATPase protein density at the plasma membrane

(Figure 1, 2). These, results suggest that SYP132 has an unexpected role in promoting the removal of H^+-ATPase proteins from plasma membrane.

Plasma membrane H^+-ATPase and SYP132 endocytosis is co-opted

The effects of the dominant negative SYP132$^{Habc\Delta}$ on H^+-ATPase traffic were supported by over-expression of the functional full-length SYP132 which promoted membrane traffic of the H^+-ATPase proteins from the plasma membrane to the internal membranes (Figure 1-4, Supplemental Figure S6) and they also lead to additional conclusions.

Qa-SNAREs which act as i-SNAREs are reported to form non-fusogenic complexes and block secretory traffic, contrary to their conventional roles in secretion (Varlamov et al., 2004). The reduction in density of the H^+-ATPase proteins at the plasma membrane in the SYP132-OX plants (Figure 1-4, Supplemental Figure S6) could be therefore attributed to the i-SNARE activity of SYP132, apparent upon the over-expression of the Qa-SNARE. However, the dominant negative SYP132$^{Habc\Delta}$, which logically must also block secretory traffic, instead augmented H^+-ATPase density at the plasma membrane (Figure 1, 2). Moreover, additional roles of SYP132 in promoting secretory traffic at the phragmoplast during cytokinesis are established (Park et al., 2018), rendering the possibility that it acts as an i-SNARE and interferes with secretory traffic unlikely.

Experiments with clathrin mutant Arabidopsis showed that SYP132-associated H^+-ATPase traffic was sensitive to clathrin (Figure 3). Biochemical analysis of fractionated membranes (Figure 4) showed that H^+-ATPase protein integration into the plasma membrane is inversely related to the levels of SYP132 expression (Supplemental Figure S7). Indeed, the *syp132*^{T} mutant plants had almost double the H^+-ATPase density compared to the wild type while the SYP132-OX plants had half as much H^+-ATPase density at the plasma membrane (Figure 4, Supplemental Figure S7). Taken together, these findings indicate an unusual role of the Qa-

581 SNARE SYP132 in promoting H^+-ATPase residence in internal membranes relative to the
582 plasma membrane.

583 SYP132 is primarily localized to the plasma membrane (Supplemental Figure S4) (Enami et
584 al., 2009). Even so, SNARE-mediated vesicle traffic for secretion at the plasma membrane
585 generally must occur in tandem with vesicle endocytosis for regulation of vesicle membrane
586 and cognate SNARE turnover (Larson et al., 2017, Karnik et al., 2013, Karnik et al., 2015).
587 Therefore, additional effects of SYP132 on post-synthesis H^+-ATPase delivery to the plasma
588 membrane or on its recycling from endosomal compartments cannot be completely ruled
589 out. Blocking H^+-ATPase forward traffic and Golgi retention following treatment with brefeldin
590 A (BFA), an inhibitor of the Golgi apparatus, affects H^+ extrusion (Lee et al., 2002, Schindler
591 et al., 1994), but SYP132 does not accumulate in BFA sensitive compartments (Ichikawa et
592 al., 2014). Thus, no compelling evidence exists for the role of SYP132 in BFA-sensitive
593 forward traffic of the H^+-ATPase proteins. Interestingly, in the SYP132-OX leaves, the
594 population of the RFP-SYP132 proteins localized to the internal membranes was higher
595 compared to the plasma membrane (Figures 1, 4). Taken together, these finding suggest
596 that traffic of the H^+-ATPases is tied with that of SYP132, and effectively this co-option of
597 traffic allows for coordination between proton transport, secretory traffic, and vesicle
598 membrane cycling.

599

600 **SYP132 affects physiology of plant growth and stomatal responses**

601 The roles of SYP132-mediated traffic in plant physiology are substantiated by phenotypes
602 corresponding to reduce plasma membrane H^+-ATPase activity; leaf apoplast pH was more
603 alkaline in the SYP132-OX compared to the wild type plants and shoot growth was reduced
604 (Figure 5, Supplemental Figure S8). In the SYP132-OX lines, reduced H^+-ATPase density at
605 the plasma membrane (Figure 4) corresponded to reduced proton pumping, an increase in
606 pH of the apoplastic fluid, and a significant decrease in plant growth (Figure 5, Supplemental
607 Figures S8 and S9). The pH of the apoplast is an important factor controlling the plasticity of

608 the cell wall and it varies rapidly and differentially between cell types during growth
609 (Palmgren, 2001, Michelet and Boutry, 1995). These observations effectively highlight the
610 roles of SYP132 in membrane traffic for regulation of density of the plasma membrane H^+-
611 ATPase proteins, which has direct consequences on the regulation of proton transport for
612 plastic cell expansion.

613 In plants, stomata are excellent models to gauge H^+-ATPase function. Blue light-induced
614 stomatal opening is mediated through activation of plasma membrane H^+-ATPases in guard
615 cells (Yamauchi et al., 2016). Moreover, stomata must open and close in response to
616 various environmental stimuli including light, humidity, and foliar pathogens (Jezek and Blatt,
617 2017, Kaundal et al., 2017, Roelfsema and Hedrich, 2005, Shimazaki et al., 2007, Shope et
618 al., 2008). Presumably, membrane traffic and function of primary transporters of guard cells,
619 such as the plasma membrane H^+-ATPases and the KAT1 K^+ channels, must be tightly
620 regulated in response to multiple environmental stimuli and stresses. The Qa-SNARE
621 SYP121 mediates recycling KAT1 K^+ channels to the plasma membrane for programmed
622 stomatal closure and the regulation of stomatal opening (Jezek and Blatt, 2017, Karnik et al.,
623 2017, Eisenach et al., 2012, Sutter et al., 2006). We found that the SYP132-OX lines
624 showed smaller stomatal apertures compared to the wild type (Figure 7), an observation
625 which we attribute chiefly to reduced H^+-ATPase density and function at the plasma
626 membrane. This semi-closed stomatal phenotype was reversed following treatment with the
627 fungal toxin fusicoccin (Figure 7), which activates the plasma membrane H^+-ATPase and the
628 KAT1 K^+ channels by stabilizing their binding with the regulatory 14-3-3 proteins (Marre,
629 1979, Saponaro et al., 2017). These observations highlight the importance of the H^+-ATPase
630 density and its regulation by SYP132 in guard cells, even if the Qa-SNARE has other roles in
631 regulation of stomatal responses.

632

633 **Plasma membrane H^+-ATPase traffic is regulated by plant hormones.**

The most striking aspect of the SYP132-mediated membrane traffic is its hormone-control. In growing shoot tissue, auxin further suppressed SYP132 transcript levels (Figure 6) and consequently, reduced the traffic of the H^+-ATPases from the plasma membrane to internal membrane compartments (Figure 8D). A marked increase in plasma membrane H^+-ATPase density was noted in previous studies (Hager et al., 1991) and can be attributed to the block of endocytic traffic by depletion of SYP132. The effect of SYP132 levels on H^+-ATPase traffic are the same in different plant tissue. Notably, differential regulation of SYP132 expression occurs in roots and shoots in the presence of high concentrations of auxin (Figure 6). Thus, depending on hormonal cues, SYP132 expression and thereby H^+-ATPase density at the plasma membrane are modulated differentially.

The stress hormone ABA regulates plasma membrane H^+-ATPase activity and in stomata, ABA drives closure to reduce water loss during drought (Jezek and Blatt, 2017, Merlot et al., 2007). Our data allow a new interpretation of recent data on ABA-mediated regulation of the H^+-ATPases. Recently, Xue et al. (2015) showed that ABA induces interactions between the plasma membrane H^+-ATPases and the R-SNARE VAMP711 for inhibition of proton pumping. However, VAMP711 is primarily localized at the tonoplast membrane (Heard et al., 2015) and it does not re-localize to the plasma membrane in response to ABA (Xue et al., 2018). This raises the possibility that ABA influences post endocytic traffic of the H^+-ATPase proteins. In our studies, density of the H^+-ATPases at the plasma membrane was substantially reduced in wild type plants in the presence of ABA, like in the SYP132-OX plants (Figure 8 A-B). Total cellular H^+-ATPase and RFP-SYP132 levels were also reduced (Figure 8 F, G). In light of these findings, we can place the hormone ABA as a promoter of H^+-ATPase endocytosis from the plasma membrane for degradation via the VAMP711 pathway to the vacuole.

An outstanding feature of SYP132-associated endocytic traffic is that it appears to be influenced by the functional status of the H^+-ATPase proteins (Figures 7 and 8). ABA promotes H^+-ATPase dephosphorylation (Zhang et al., 2004, MacRobbie, 1991, Meckel et

al., 2004) for inactivation of proton pumping. H^+-ATPase endocytosis is favored in presence of ABA (Figure 8). Conversely, fusicoccin locks the H^+-ATPase proteins in their active state (Marre, 1979, Saponaro et al., 2017) and in SYP132-OX plants, H^+-ATPase endocytosis from the plasma membrane was reduced following fusicoccin treatment (Figures 7 and 8). Thus, for SYP132, we consider the possibility that hormonal regulation of membrane traffic associated with this Qa-SNARE coordinates with H^+-ATPase activity at various levels within the plant. Further research will help dissect the complexities of SYP132-associated traffic and its regulation during hormone crosstalk.

CONCLUSIONS

In summary (see Figure 9 for a model), we uncover a mechanism of co-option of the Qa-SNARE and the plasma membrane H^+-ATPase in vesicle traffic to maintain a steady turnover of H^+-ATPase proteins at the plasma membrane for active function. Traffic of active H^+-ATPase proteins at the plasma membrane is blocked to maintain proton extrusion, while inactivation of the H^+-ATPases promotes their removal from the plasma membrane. Thus, control of H^+-ATPase traffic is an important counterpart to its post-translational regulation. We identify SYP132 and the endocytosis of the H^+-ATPases as novel and dominant elements of this regulation which, in normal conditions, serves to maintain the functional pool of H^+-ATPases at the plasma membrane. Plant hormones, including auxin and ABA, govern SYP132-associated traffic in conjunction with their regulation of the H^+-ATPases for plant growth and morphogenesis. It will be of interest now to pursue these findings in relation to H^+-ATPase traffic in specialized tissues such as the growing pollen tubes (Certal et al., 2008), where these proteins are locally excluded from the growing tip. Interestingly, a proteomics screen for the Arabidopsis SYP132 interactome has identified the H^+-ATPase proteins as one of the SNARE binding partners (Fujiwara et al., 2014). Indeed, some interesting interactions of trafficking SNAREs with non-SNARE proteins are noted to affect cellular traffic and plant physiology (Honsbein et al., 2009, Barozzi et al., 2018, Faraco et al.,

688 2017). We are currently investigating the dynamics of SYP132 interactions and their
689 relationship to H^+-ATPase traffic as well as the physiology of plant growth. Our studies
690 launch an exciting future research focus on hormone-regulation of membrane traffic for plant
691 growth and morphogenesis.

MATERIALS AND METHODS

Plasmid construction

Arabidopsis (*Arabidopsis thaliana*) SYP132, SYP132$^{Habc\Delta}$, and AHA1 were PCR amplified from cDNA and recombined using Gateway™ cloning (Invitrogen) to prepare entry clones in pDONR207, pDONR221–P1P4 or pDONR221–P3P2 vectors (Grefen and Blatt, 2012). Supplemental Table S1 lists all primers used for cloning in the study. SYP121 entry clone was from previous work (Karnik et al., 2013, Zhang et al., 2015).

For balanced co-expression of proteins in plants, we used the Gateway™ based 2in1 vector system, specifically the pFRET-2in1gc-NN vector (Hecker, 2015) to drive co-expression of GFP or mCherry fusion proteins, each under the *Cauliflower* mosaic virus (*Ca*MV) 35S promoter. For GFP-, RFP-, or YFP- fused SYP121, SYP132, SYP132$^{Habc\Delta}$, and AHA1 protein expression under the *Ca*MV 35S promoter in plants, constructs with Basta™ or kanamycin resistance for selection were cloned in Gateway™ based vectors (Karimi et al., 2002).

Plant growth and transformation

Agrobacterium tumefaciens GV3101 carrying the desired constructs as described previously (Tyrrell et al., 2007) was used for all transient and stable plant transformations. Wild type tobacco (*Nicotiana tabacum*) plants were grown in soil at 26°C and 70% relative humidity on a 16-h-day/8-h-night cycle. 4 to 6 weeks old plants with three to four fully expanded leaves were selected for transient transformation of the leaf epidermis by infiltration with *Agrobacteria* carrying the desired constructs as described previously (Karnik et al., 2013, Karnik et al., 2015, Zhang et al., 2015). Transgenic stable lines of Arabidopsis ecotype Columbia-0 (wild type) expressing GFP or RFP-fused SYP132 (SYP132-OX), YFP-SYP121 (SYP121-OX), and 35S:*GFP-AHA1* (AHA1-OX) (Hashimoto-Sugimoto et al., 2013) co-expressing SYP132 (GFP-AHA1/RFP-SYP132) were generated by floral dip (Clough and

718 Bent, 1998). As described previously (Karnik et al., 2015), ≥ three independent transformed
719 lines were selected on 50µg ml^{-1} Basta™ (phosphinothricin, Bayer Crop Science) or 50µg
720 ml^{-1} kanamycin (Harrison et al., 2006). Plants grown from T3 or T4 generation seeds of three
721 independently transformed lines for each transgenic Arabidopsis line were analyzed in detail
722 and two lines, each, showing similar fluorophore-fused-protein expression in immunoblot
723 analysis were used for experiments. T-DNA insertion lines were analyzed by PCR
724 genotyping to identify (http://signal.salk.edu/cgi-bin/tdnaexpress) heterozygous *syp132*^{T}
725 (*At5g08080*, SAIL 403_B09) mutants as described in (Park et al., 2018). Primers are listed in
726 Supplemental Table S2.

727

728 **Plant treatments and phenotype analysis**

729 Phenotypic analysis was carried out with each of the two independently transformed
730 transgenic lines for GFP- and RFP- fused SYP132; (35S: GFP-SYP132: 1-1, 35S: GFP-
731 SYP132: 3-1, 35S: RFP-SYP132: 1-1, and 35S: RFP-SYP132: 2-4). For simplicity, main
732 Figures show only RFP-SYP132: 2-4 as a representative.

733 *Shoot growth analysis:* Arabidopsis plants were grown in standard conditions on soil under
734 8-hr-light/ 16-h-dark, 18/22°C (light/dark) cycle with 150 µmol m^{-2} s^{-1} PAR light, 55%
735 restricted humidity for biochemistry and stomatal aperture experiments. For shoot growth
736 analysis, plants were grown on soil under short day 8-h-light/16-h-dark or long day 16-h-
737 light/ 8-h-dark (light/dark) cycle for three weeks as in (Karnik et al., 2015).

738 *Hypocotyl elongation:* Seeds were sterilized and placed on half-strength MS medium
739 (Sigma-Aldrich) containing 0.8% (w/v) agar and 0.5% (w/v) sucrose and following
740 stratification for three days at 4°C. Seed germination was activated by placing the plates
741 under a red filter for two hours and then allowed to grow vertically in the dark for four days.
742 Plates were scanned, and length of the etiolated hypocotyls was measured using the Fiji
743 (NIH) software (Schindelin et al., 2012).

744 *Apoplast wash fluid pH:* Rosette leaves of three-week-old Arabidopsis plants were infiltrated
745 with water and immediately cut into 5-6 mm wide strips. The strips were bundled, rolled, and
746 loaded vertically (cut ends top and bottom) in microfuge spin columns; apoplast fluid was
747 flushed out by centrifugation (three minutes at 18K rpm) (Grefen et al., 2015). Fluid from
748 three different leaves from each plant was pooled and pH was measured using a micro pH
749 electrode.

750 *Stomatal aperture measurements:* Rosette leaves were obtained from four-week-old plants
751 grown on soil under 8-hr-light/ 16-h-dark, 18/22°C (light/dark) cycle with 150 µmol m^{-2} s^{-1}
752 PAR light, 55% restricted humidity. Intact leaf stomatal pores were stained with propidium
753 iodide (PI) for imaging to measure stomatal aperture as described in (Chitrakar and Melotto,
754 2010). Treatments were with control (0.02% [v/v] ethanol in water), with 10 µM Fusicoccin
755 (Hashimoto-Sugimoto et al., 2013), or with 5 µM ABA (Merlot et al., 2007), for two hours.

756 *Samples for imaging:* Imaging of transiently transformed *Nicotiana tabacum* plants was
757 carried out two days following transformation using leaf sections infiltrated with water or with
758 1M NaCl for plasmolysis.

759 Three-day-old wild type or 35S: GFP-AHA1 Arabidopsis seedlings grown in sterile liquid
760 0.05x MS medium were transiently transformed with *Agrobacterium tumefaciens* as
761 described previously (Grefen et al., 2010). Imaging of root hair was carried out two days
762 following the transformation of seedlings.

763

764 **Genotyping and reverse transcription quantitative PCR analysis**

765 *Plant growth and sample preparation:* Surface-sterilized Arabidopsis seeds were vernalized
766 for two-three days at 4°C. Seedlings were grown vertically at 22°C and 150 µmol m^{-2} s^{-1}
767 under a 16-h light/8-h dark cycle on half-strength MS media supplemented with 0.5% (w/v)
768 sucrose and 0.8% (w/v) agar. 5-7 days after germination, seedling shoots and roots were
769 separated by cutting with a scalpel and incubated separately in liquid half-strength MS or

half-strength MS supplemented with 10^{-6} M NAA for 60 and 180 minutes. ~100 roots/ sample were collected by flash freezing in liquid N_2.

RNA isolation and RT-qPCR: Total RNA was extracted and purified by TRIzol™ Plus RNA purification kit (Invitrogen) as per the supplier's manual. 1 µg of total RNA from each sample was used to the synthesis of cDNA using Quanti Tect Reverse Transcription Kit (QIAGEN). Reverse transcription quantitative real-time PCR (RT-qPCR) was performed with Brilliant III Ultra-Fast SYBR® Green qPCR Master Mix (Agilent) as per manufacturer's recommendation in Step One Plus™ Real-Time PCR System (Thermo Fisher, USA). The gene-specific primer pairs are listed in Supplemental Table S3. Relative gene expression was calculated ($2^{-\Delta CT}$ method) with the mitochondrial 18S rRNA (*AtMg01390*) as the reference gene. Fold change in gene expression following NAA was calculated as $2^{(-\Delta\Delta CT)}$ (Livak and Schmittgen, 2001). Primers, as described in (Enami et al., 2009), are listed in Supplemental Table S3.

Confocal imaging

Confocal images of *N. tabacum* epidermis and Arabidopsis root hair were collected using a Leica TCS SP8-SMD confocal microscope with spectral GaAsP detectors. Images were collected using the 40x/0.75NA and 63x/0.75NA oil immersion objective lenses, respectively. For secretory traffic assay, images were acquired from tobacco epidermis using the 20x/0.75NA air objective. GFP fluorescence was excited with continuous 488nm or 20MHz-pulsed 470nm light and collected over 500-535nm. mCherry fluorescence was collected over 590-645nm following excitation at 552nm. RFP was excited with 552nm light and RFP fluorescence emission was collected over 560-615nm. FM4-64 was excited using the 488nm laser line, and emission was collected over 750-780nm. For stomatal aperture measurements, imaging of lower surface of the leaves was carried out as described in (Chitrakar and Melotto, 2010) using a 20x/0.75NA air objective lens to detect the fluorescence of propidium iodide by excitation at 453nm and emission at 543-620nm.

Quantification of fluorescence distribution

Cell periphery/ internal fluorescence distribution: To quantify the distribution of the fluorophore fused proteins between the cell periphery and its interior, transiently transformed tobacco epidermis cells were plasmolysed with 1M NaCl to retract the plasma membrane and resolve cell interior. Confocal images were collected as Z-stacks and rendered as 3D projections (Supplemental Figure S1) prior to analysis. For each cell, ROIs demarcating cell periphery (width ~1.5 µM) and cell interior were traced using the bright field image overlay as reference. Integrated fluorescence density was measured using Fiji (NIH) software for each ROI and corrected for background fluorescence using the equation [Corrected total fluorescence= Integrated Density–(Area of selected ROI x Mean fluorescence of background)], described in (Marwaha and Sharma, 2017). Proportion of fluorophore distribution at the cell periphery and interior was represented as bar graphs of means periphery/internal fluorescence ratios.

Fluorescence distribution in cell interior: To quantify the proportion of internalization in root hair cells, an outline was drawn to define cell interior using the rectangular selection tool and the brightfield image for reference. Also, the region of cell periphery was defined by tracing a ~1.5 µm wide line using the brightfield image as reference. Mean fluorescence was measured for each region and ratioed as internal/periphery, as a measure of internalization, which was plotted as bar graphs and accounted for the expression levels for each fluorophore in the cells.

Fluorescence distribution at cell periphery for puncta: To quantify the proportion of fluorophore-tagged protein that distribute to puncta the percent relative standard deviation (%RSD) analysis was used as described in (Eisenach et al., 2014). Briefly, the %RSD of intensities determined from a 1-pixel-wide line around the periphery of plasmolysed cells using the bright field image as reference were measured using Fiji (NIH) and normalized to the intensity means.

Membrane Fractionation Two-Phase System

Microsomal membrane isolation and aqueous two-phase partitioning were conducted based on modified procedures (Advani et al., 1999, Yang and Murphy, 2013, Yoshida et al., 1983, Alexandersson et al., 2008). Briefly, freshly harvested four-week-old Arabidopsis rosettes were ground with mortar and pestle in homogenization buffer [330 mM Sucrose, 25 mM HEPES-KOH, pH 7.5, 5 mM EDTA-KOH, 0.2% (w/v) BSA, 0.6% PVP (Polyvinylpyrrolidone, PVP40, Sigma-Aldrich), 5 mM DTT, 5 mM Ascorbic acid, 0.5 mM PMSF (Phenylmethylsulphonyl fluoride), Protease inhibitor (Thermo Fisher Scientific)]. The homogenates were filtered through Miracloth (Merck) and then centrifuged at 8,000g at 4°C for 15min. Microsomal pellets were collected by centrifugation of supernatants at 100,000g at 4°C for 1h and resuspended with Resuspension buffer (Buffer R, 330 mM Sucrose, 5 mM Potassium phosphate (mixture of 200 mM KH_2PO_4 and 20 0mM K_2HPO_4, pH 7.8), 0.1 mM EDTA-KOH, 0.1 mM EGTA, 1 mM DTT, Protease inhibitor cocktail, 100 mM PMSF). Resuspended microsomal membranes were added to a 27 g phase buffer (6.5% [w/v] Dextran T500, 6.5% [w/v] PEG3350, 330 mM sucrose, 5 mM Potassium phosphate, 3 mM KCl) and phases were collected separately at 1,500g at 4°C for 15 min. Upper and lower phases were repartitioned twice with fresh lower or upper phase (without membranes). Purified phases were diluted with Buffer R in three-fold for upper phases and 10-fold for lower phases. Plasma (upper) and internal (lower) membranes were collected by centrifugation at 100,000g, 4°C for 1 h and resuspended in Buffer R. Protein quantity was determined using Bradford (Bio-Rad) with BSA Fraction V as a standard.

Immunoblot

Sample preparation: Plant samples for immune blot were prepared as described in (Karnik et al., 2015). Briefly, plant leaves were excised and flash-frozen in liquid N_2. Frozen tissue was

849 ground in equal volumes (w/v) of homogenization buffer (HB) containing 500 mM sucrose,
850 10% (v/v) glycerol, 20 mM EDTA, 20 mM EGTA, Protease Inhibitor (Roche), 10 mM ascorbic
851 acid, 5 mM DTT, and 50 mM Tris-HCl, pH 7.4, and centrifuged at 13,000g and 4°C for 30
852 min to pellet debris. Supernatant was diluted to 10 µg/µl in HB and mixed 1:1 with Laemmli
853 buffer containing 2.5% (v/v) 2-mercaptoethanol, heated to 95°C for 10 min, and separated
854 by SDS-PAGE. Proteins from yeast were prepared as described previously (Grefen et al.,
855 2010a). All samples were diluted in loading buffer to 5 mg protein/ml per lane. Ponceau S-
856 stained Rubisco bands were used as loading standards for plant samples.

857

858 *Immunoblot:* Nitrocellulose membranes with transferred separated proteins were first probed
859 with primary antibodies: anti-GFP (1:5,000 dilution; Abcam), anti-mCherry (1:5,000 dilution;
860 Abcam), anti-H^+-ATPase (1:2,500 dilution; Agrisera), anti-KAT1 (1:500 dilution, Agrisera),
861 anti-BiP; luminal-binding protein (1:2,500 dilution, Agrisera), and anti-YFP (1:3,000 dilution;
862 Agrisera). Subsequently, secondary antibody goat anti-rabbit-HRP conjugate (1:20,000
863 dilution, Abcam) was used. Cross-reacting bands were visualized using West Femto Super
864 Signal® chemiluminescence detection (Thermo Pierce) and imaged by Fusion
865 Chemiluminescence imager (Peqlab). In the 2-phase experiments, membranes were cut in
866 the middle to probe with separate set of antibodies on the same membrane for detection of
867 proteins with significant differences in molecular weight. In some experiments, membranes
868 were re-probed after stripping in 100 mM β-mercaptoethanol, 2% (w/v) SDS, and 62.5 mM
869 Tris-HCl, pH 6.7, at 50°C for 15 min. For comparative analysis of immunoblot band density,
870 densitometry data was normalized against corresponding total protein density for each gel
871 lane by Coomassie stain.

872

873 *Immunoblot analysis:* Immunoblot band intensities in each lane for different proteins were
874 measured using Fiji (NIH) gel analysis plug-in and normalized against the intensity of

corresponding loading controls. Mean band intensity data was calculated and statistically analysed from n=3 experiments and plotted as a measure of protein density.

GPI signal peptide-anchored split-ubiquitin (GPS) system

Protein-protein interactions for SYP132$^{\Delta C}$ and SYP132 $^{Habc\Delta}$ as baits in vector pEXG2Met-Dest and SYP132, VAMP721, and SNAP33 as prey in vector pNX35-Dest (Grefen et al., 2009). The GPS assay was performed as described in (Zhang et al., 2018). The bait constructs were transferred in yeast strain THY.AP4 and prey constructs were transferred in THY.AP5. 10 to 15 yeast colonies were selected and inoculated into selective media (CSM_{-LM} for THY.AP4 and CSM_{-TUM} for THY.AP5) for overnight growth at 180 rpm and 28°C. Liquid cultures were harvested and resuspended in YPD medium. Yeast mating was performed in sterile PCR tubes by mixing equal aliquots of yeast containing bait and prey construct. Aliquots of 5 µl were dropped on YPD plates and incubated at 28°C overnight. Then colonies were transferred from YPD onto CSM_{-LTUM} plates and incubated at 28°C for 2-3 days. Diploid colonies were selected and inoculated in liquid CSM_{-LTUM} media and grown at 180 rpm 28°C overnight. Then the yeast was harvested and resuspended in sterile water. Serial dilutions at OD_{600} 1.0 and 0.1 in water were dropped on $CSM_{-AHLTUM}$ plates (5 µL per spot) with methionine added at increasing concentrations. Plates were incubated at 28°C and images were taken after three days. Yeast was also dropped on CSM_{-LTUM} control plates to confirm mating efficiency and cell density and growth was imaged after 24 h at 28°C. To verify expression, yeast was harvested and extracted for protein gel blot analysis using anti-HA antibody (Roche) for prey and anti-VP16 antibody (Abcam) for bait.

STATISTICAL ANALYSIS

Data are means ± SE of n≥3. Statistical analysis was performed using Sigmaplot 11.2 (Systat Software, San Jose, CA). Significance was determined by Student's T-test or ANOVA using Holm-Sidak method for all pairwise multiple comparisons, $p<0.05$.

ACCESSION NUMBERS

Transgenic lines used in the study are: for CHC1 (At3g11130) T-DNA mutants: *chc1-1* (SALK_112213) and *chc1-2* (SALK_103252). SYP132 T-DNA mutant (*syp132*^{T}): SAIL_403_B09. Sequence data from work can be found in the *Arabidopsis thaliana* Genome Initiative or GenBank/EMBL databases under the accession numbers: AHA1 (*At2g18960*), SYP121 (*At3g11820*), SYP123 (*At4g03330*), SYP132 (full length) (*At5g08080.1*), SYP132$^{Habc\Delta}$ (*At5g08080.2*), VAMP721 (*At1g04750*), SNAP33 (*At5g61210*), SBT5.2 (*At4g30270*), MERI5 (*At1g20160*) and KAT1 (*At5g46240*).

SUPPLEMENTAL DATA

Supplemental Figure S1. SYP132 affects AHA1 distribution in *Nicotiana tabacum* epidermal cells.

Supplemental Figure S2. Domain organisation of dominant negative SYP132$^{Habc\Delta}$ and its interactions with cognate SNAREs.

Supplemental Figure S3. Dominant negative SYP132$^{Habc\Delta}$ affects SYP132-dependent secretory traffic at the plasma membrane.

Supplemental Figure S4. Qa-SNARE localization at the plasma membrane.

Supplemental Figure S5. SYP132 does not affect distribution of KAT1 puncta.

Supplemental Figure S6. Stable SYP132 over-expression affects AHA1 internalization.

Supplemental Figure S7. SYP132 protein and mRNA transcript expression in transgenic over-expression and mutant *Arabidopsis thaliana* lines.

Supplemental Figure S8. Independently transformed transgenic SYP132-OX Arabidopsis lines have similar phenotypes.

Supplemental Figure S9. Increased AHA1 density at the plasma membrane promotes shoot growth.

Supplemental Figure S10. Immunoblots of membrane fractions following treatment with plant hormones and fungal toxin fusicoccin.

930 Supplemental Figure S11 Immunoblots for transient transformations to verify protein
931 expression.

932 Supplemental Table S1. Primers used in molecular cloning.

933 Supplemental Table S2. List of primers used for genotyping.

934 Supplement Table S3. List of primers used for RT-qPCR.

935 Supplemental Table S4. Binding efficiency of primers used in RT-qPCR.

936

937 **MATERIALS AND CORRESPONDENCE**

938 35S:*GFP*-AHA1 seeds (Hashimoto-Sugimoto et al., 2013) were a kind gift from Koh Iba lab.
939 Clathrin mutant CHC1 and HUB1 seeds (Larson et al., 2017), the 2in1 and plant expression
940 plasmids (Karnik et al., 2015), entry clones for KAT1 and SYP121 and all constructs for
941 secretory traffic assay (Waghmare et al., 2018) were gifts from Mike Blatt lab.

942

943 **DATA AVAILABILITY**

944 Vectors are available at www.psrg.org.uk

945

946 **Acknowledgements**

947 We are grateful to Professor Mike Blatt for critical reading of the manuscript. We thank
948 Amparo Ruiz-Prado for help with the logistics of plant propagation.

949

950 **Competing interests**

951 Authors have no competing interests.

952

953 **Figure Legends**

Figure 1. Effect of plasma membrane Qa-SNAREs on cellular AHA1 localization.

(A) Localization pattern in *Nicotiana tabacum* epidermal cells transiently transformed using the bicistronic pFRET-2in1gc-NN vector, to express mCherry-fused AHA1 on its own or with GFP-fused Qa-SNAREs SYP121, SYP132 and SYP132$^{Habc\Delta}$. Confocal images of the epidermal cells were acquired on a single focal plane. Representative (left-right) images for fluorescence, GFP-Qa-SNARE (green) overlay with chlorophyll (blue), mCherry-AHA1 (red) with chlorophyll (blue) and overlay with brightfield. Scale bar = 20 µm. Immunoblots (right hand panels) to verify expression of the Qa-SNAREs and AHA1 with anti-GFP and anti-mCherry antibodies respectively (see Supplemental Figure S11A). (**B**-**D**) Bar graphs show mean of cell periphery/internal fluorescence ratios ± S.E, n≥12; (**B**) for Qa-SNAREs (RFP-fused) expressed on their own (see Supplemental Figure S4), (**C**) for Qa-SNAREs (GFP-fused) co-expressed with AHA1 and (**D**) for AHA1 (mCherry-fused) expressed on its own (none) or with the Qa-SNAREs. Cells were plasmolysed with 1M NaCl to retract the plasma membrane resolve the cell interior. Images were collected as Z-stacks and rendered as 3D projections (Supplemental Figure S1) prior to analysis. Region of cell periphery, ~1.5 µm width, and cell interior were traced for each cell using the brightfield image as reference. Integrated fluorescence density within the regions of interest was measured and corrected for background fluorescence (see Methods). Statistically significant differences using ANOVA are indicated with different letters (P<0.001).

Figure 2. SYP132 affects AHA1 integration into the plasma membrane.

(A) Localization pattern in root hair from three-day-old 35S:*GFP-AHA1 Arabidopsis thaliana* seedlings (Hashimoto-Sugimoto et al., 2013) stably expressing GFP-AHA1 were transformed with empty vector (control) or RFP-fused SYP121, SYP132 and SYP132$^{Habc\Delta}$ under the *Cauliflower* mosaic virus (*Ca*MV) 35S promoter (Karimi et al., 2002) and stained with 3µM FM4-64 (5 min, ice) to label the plasma membrane. Seedlings were washed in growth medium prior to imaging. Representative single-plane confocal images of root hairs show (left to right) florescence GFP-AHA1 (green), GFP-AHA1 (green) overlay with FM4-64 (pink), GFP-AHA1 (green) and FM4-64 (pink) overlay with bright field and the GFP-AHA1 (green) overlay with RFP-SYP (red, ~7% bleed through from FM4-64). Immunoblots on the right verify expression of the GFP-AHA1 and the RFP-SYPs using anti-GFP and anti-RFP antibodies respectively (see Supplemental Figure S11B). Yellow line and lollipop marks a representative region of the root hair membrane across which fluorescence intensities for GFP (black line) and FM4-64 (pink line) were plotted (Sklodowski et al., 2017). Scale bar = 5 µm. (**B**) Plots of GFP-AHA1 and FM4-64 fluorescence overlap in the line scan across the

membrane, represented by a yellow line and lollipop in **A**. Round insets are enlarged sections of the root hair image in **A**, marking a representative line scan region. (**C**) Peak area shaded pink represents FM4-64 and GFP-AHA1 overlap, grey area with pink outline represents lack of FM4-64 overlap, represented schematically on the bottom right. Bar graphs plot percent of total FM4-64 that overlaps with GFP-AHA1. Plots are mean values $\pm$ S.E from ≥20 root hair. Statistically significant differences using ANOVA are indicated with letters (P<0.0.05).

Figure 3. Block of clathrin function perturbs SYP132-associated internalization of AHA1.

A, C and **E** show representative confocal images of root hair from wild type and clathrin mutant Arabidopsis lines *chc1* and HUB1 (+ 2μM hydroxytamoxifen, for 48hr). Images represent florescence FM4-64 (pink), mCherry-AHA1 (red) and GFP-132 (green). Scale bar = 5 μm, arrows (white) mark intracellular accumulation. (**A**) At the plasma membrane, to test for endocytosis in the wild-type seedlings and block of clathrin mediated endocytosis in the *chc1* and HUB1 lines, seedlings were stained with 3μM FM4-64 for 5 minutes and washed in growth medium prior to imaging after 30 minutes. (**C, E**) Wild-type, *chc1* and HUB1 seedlings were transiently transformed using the pFRET-2in1gc-NN vector to express mCherry-fused AHA1 on its own (**C**) or with GFP-fused SYP132 (**E**). Bottom panels in (**C**) and right hand panels in (**E**) show immunoblots with anti-mCherry or anti-GFP antibodies to verify expression of the AHA1 and the SYP132 respectively (see Supplemental Figure S11C-D). **B**, **D** and **F** Graphs represent mean internal vs periphery fluorescence ratio following background subtraction. Region along cell periphery, ~1.5 μm width, and the cell interior were traced for each cell using the brightfield image as reference. Representative region for internal fluorescence measurement is shown with a white dotted line in (A), middle panel. Measurements were obtained for FM4-64 (**B**), mCherry-AHA1 (**D**) and GFP-SYP132 or mCherry-AHA1 (**F**). Mean values $\pm$ S.E are plotted from n≥20 root hair. Letters indicate statistically significant differences using ANOVA (P<0.001).

Figure 4. SYP132 over-expression re-localizes plasma membrane H^+-ATPases into internal membranes.

(A) Immunoblots of microsomal membrane (total), plasma membrane (PM), internal membrane (IM) and soluble (cytosol) fractions purified (see Methods) from rosette leaves of wild type, *syp132*^{T} and SYP132-OX *Arabidopsis thaliana*. Proteins were resolved on a single

gradient gel (4-20% SDS-PAGE) and specific proteins were visualised by immunoblots using antibodies; anti-H^+-ATPase (AHA, ~95 kDa, first panel), anti-RFP (RFP-SYP132, ~61 kDa, second panel), anti-BiP (Lumenal-binding protein, ~73 kDa, third panel) and anti-KAT1 (KAT1 K^+ channel, ~78 kDa, fourth panel). Total protein for each gel lane detected using Coomassie stain (bottom last panel) was used for quantitative analysis. Black lines (left) indicated position of molecular weight markers, black arrows (right) indicate expected band position. Based on band intensities for KAT1, ~96% of the marker appeared in the PM fractions and for BiP, ~95% of the marker appeared in the IM fractions, suggesting membrane fraction purity in excess of 95%. (**B**) Relative AHA distribution in the PM, IM and cytosol fractions of wild type, *syp132*^{T} and SYP132-OX leaves quantified from immunoblots using the Fiji software. (**C**) Relative RFP-SYP132 distribution in PM, IM and cytosol fractions of SYP132-OX leaves. (**D**) Relative AHA density in microsomal membranes (total) of wild type, *syp132*^{T} and SYP132-OX Arabidopsis. Data are mean ± S.E from n≥3 independent experiments. Statistical significance using ANOVA is indicated by letters (P<0.05).

Figure 5. Modulation of SYP132 expression alters H^+-ATPase function and plant growth.

(A) pH of apoplast wash fluid eluted in water was measured (see Methods) from three-week-old wild type, *syp132*^{T} and SYP132-OX *Arabidopsis thaliana* leaves. Apoplast wash fluid from three different leaves from each plant was pooled and pH was measured using a micro pH electrode. Mean $_{\pm S.E}$ data, n≥10 plants. Statistical significance using ANOVA is indicated by letters (P<0.05). **B-C** Mean $_{\pm S.E}$ values from ≥30 plants each of wild type, *syp132*^{T} and SYP132-OX *Arabidopsis thaliana* grown in 8hr light for three weeks before measurement of shoot fresh weight (**B**) and rosette area (**C**). Values are normalized to the wild type and statistical significance is indicated by letters (P<0.001). **(D)** Photographs of three-week-old wild type, *syp132*^{T} and SYP132-OX *Arabidopsis thaliana* rosettes grown in 8hr light. Immunoblots with anti-RFP antibodies to verify expression of the RFP-SYP132. Scale bar = 1 cm. **E-F** Mean $_{\pm S.E}$ data of shoot fresh weight (**E**) and rosette area (**F**) from ≥30 three-week-old wild type, *syp132*^{T} and SYP132-OX *Arabidopsis thaliana* grown in 16hr light. Values are normalized to the wild type and statistical significance is indicated by letters (P<0.05). **(G)** Three-week-old wild type, *syp132*^{T} and SYP132-OX *Arabidopsis thaliana* grown in 16hr light. Scale bar = 1 cm. Images for rosettes are digitally extracted using Image J. **(H)** Mean $_{\pm S.E}$ hypocotyl length in wild type, *syp132*^{T} and SYP132-OX *Arabidopsis thaliana* measured from four-day-old dark-grown seedlings (≥30). Independently transformed SYP132-OX lines all showed similar phenotypes (Supplemental Figure S9). Statistical significance using ANOVA is indicated by letters (P<0.001).

Figure 6. The phytohormone auxin regulates *SYP132 expression* levels.

qRT-PCR analysis relative to mitochondrial 18s rRNA (AtMg01390) expression as reference on whole plant or separated shoot and root tissue from 5-7 days old *Arabidopsis thaliana*. (**A**) Relative *SYP121*, *SYP123* and *SYP132* expression ($2^{-\Delta Ct}$) in shoot and root tissue. Data are mean ± S.E, representative of three biological replicates. **B-C** Fold change in *SYP121*, *SYP123* and *SYP132* expression ($2^{-\Delta\Delta Ct}$) (Livak and Schmittgen, 2001) compared to control (0.02% [v/v] ethanol in water), upon treatment with 10^{-6}M NAA for 60 minutes (grey bars) and 180 minutes (black bars) in shoots (**B**) and roots (**C**). Mean values ± S.E representative of three biological replicates are plotted. * indicates statistically significant differences compared to the control, using Student's t-test ($P<0.001$); fold change reference (1.0) marked with a dotted line. Since the data were either not normally distributed or had unequal variances, a Kruskal-Wallis ANOVA on ranks was undertaken and a pairwise comparison using Dunn's method was applied. Letters denote statistically significant differences ($P<0.001$).

Figure 7. Modulation of SYP132 expression affects stomatal aperture.

Steady state, intact leaf stomatal apertures in four-week-old wild type, *syp132*^{T} and SYP132-OX *Arabidopsis* following treatment with control (0.02% [v/v] ethanol in water) and 10^{-5} M fusicoccin (FC) for two hours. Data are mean ± S.E apertures from ≥100 stomata from three independent experiments measured using the Fiji (NIH) software. Statistical significance using ANOVA is indicated by letters ($P<0.05$).

Figure 8. Plasma membrane H^{+}-ATPase traffic is under the control of plant hormones and fungal toxin fusicoccin.

(A) Immunoblot analysis of leaf microsomal fractions (total), purified plasma membrane (PM) and internal membrane (IM) fractions of wild type (top), and SYP132-OX (bottom) *Arabidopsis thaliana*. PM and IM fractions were estimated to be ~95% pure (see Supplemental Figure S10). Bands (AHA, ~95kDa and RFP-SYP132, ~61kDa) were resolved on a single gel for immunoblot with anti-H^{+}-ATPase and anti-RFP antibodies. Leaves were infiltrated with control (0.02% [v/v] ethanol in water), 10^{-5}M fusicoccin (FC), 10^{-6}M NAA and 10^{-5}M ABA for two hours before fractionation of membranes by phase partitioning (see Methods). Total protein for each gel lane stained using Coomassie stain (bottom last panel) used for quantitative analysis. **B-C** Plasma membrane density relative to wild type control for

H^+-ATPase (**B**) and relative to SYP132-OX control treatment for RFP-SYP132 (**C**). **D-E** Ratio of plasma membrane to internal membrane density for H^+-ATPase (**D**) and RFP-SYP132 (**E**). **F-G** Total expression levels of the plasma membrane H^+-ATPase relative to wild type control for H^+-ATPase (**F**) and relative to SYP132-OX control for RFP-SYP132 (**G**). All data represent mean $\pm$ S.E from three independent experiments. Statistical significance using ANOVA is indicated by letters ($P<0.05$).

Figure 9. Model of SYP132-associated plasma membrane H^+-ATPase traffic controlled by hormones.

Net population of the H^+-ATPase proteins at the plasma membrane reflects a balance of their exocytosis, endocytosis and recycling. SYP132 affects H^+-ATPase protein distribution between the plasma membrane and internal membrane compartments. Panel (**A**) encapsulates H^+-ATPase membrane traffic in normal growth conditions. Clathrin mediated endocytosis (CME) of the H^+-ATPase proteins from the plasma membrane in association with the low abundant SYP132 is balanced by recycling and exocytotic delivery of the newly synthesised proteins (omitted for simplicity). The population of H^+-ATPase proteins at the plasma membrane includes both inactive (dark green) and the active (light green with red outline) pump proteins. Panel (**B**) Growth hormone auxin suppresses SYP132 expression and consequently SYP132-associated H^+-ATPase traffic at the plasma membrane is reduced. Both density and activity of H^+-ATPase proteins at the plasma membrane are augmented allowing an increase in proton (H^+) extrusion into the apoplast due to auxin. Panel (**C**) Stress hormone abscisic acid (ABA) promotes SYP132-associated traffic of the H^+-ATPases directed to the vacuole for degradation. Co-opted with the H^+-ATPases, the SYP132 protein density at the plasma membrane is reduced due to ABA and H^+ extrusion to apoplast is suppressed. Panel (**D**) Fungal toxin fusicoccin induces H^+-ATPase activation by stabilizing the binding of H^+-ATPase proteins with regulatory 14-3-3 proteins (blue crescent). Our hypothesis is that SYP132-associated endocytosis of the 'active' H^+-ATPase is blocked upon fusicoccin treatment and consequently density of H^+-ATPase and SYP132 proteins at the plasma membrane is augmented. In summary, H^+-ATPase traffic from the plasma membrane is under the control of hormones and is un-expectedly co-opted with a secretory Qa-SNARE SYP132; affecting vegetative plant growth and morphogenesis. Dashed arrows indicate direction of traffic to and from the plasma membrane, circles with line through the centre indicate 'block' of traffic.

REFERENCES

ADVANI, R. J., YANG, B., PREKERIS, R., LEE, K. C., KLUMPERMAN, J. & SCHELLER, R. H. 1999. VAMP-7 mediates vesicular transport from endosomes to lysosomes. *Journal Of Cell Biology,* 146**,** 765-775.

ALEXANDERSSON, E., GUSTAVSSON, N., BERNFUR, K., KARLSSON, A., KJELLBOM, P. & LARSSON, C. 2008. Purification and proteomic analysis of plant plasma membranes. *Methods Mol Biol,* 432**,** 161-73.

ARANGO, M., GEVAUDANT, F., OUFATTOLE, M. & BOUTRY, M. 2003. The plasma membrane proton pump ATPase: the significance of gene subfamilies. *Planta,* 216**,** 355-65.

ASSAAD, F. F., QIU, J. L., YOUNGS, H., EHRHARDT, D., ZIMMERLI, L., KALDE, M., WANNER, G., PECK, S. C., EDWARDS, H., RAMONELL, K., SOMERVILLE, C. R. & THORDAL-CHRISTENSEN, H. 2004. The PEN1 syntaxin defines a novel cellular compartment upon fungal attack and is required for the timely assembly of papillae. *Molecular Biology Of The Cell,* 15**,** 5118-5129.

BAROZZI, F., PAPADIA, P., STEFANO, G., RENNA, L., BRANDIZZI, F., MIGONI, D., FANIZZI, F. P., PIRO, G. & DI SANSEBASTIANO, G. P. 2018. Variation in Membrane Trafficking Linked to SNARE AtSYP51 Interaction With Aquaporin NIP1;1. *Front Plant Sci,* 9**,** 1949.

BASSHAM, D. C. & BLATT, M. R. 2008. SNAREs: Cogs and Coordinators in Signaling and Development. *Plant Physiology,* 147**,** 1504-1515.

BOCK, J. B., MATERN, H. T., PEDEN, A. A. & SCHELLER, R. H. 2001. A genomic perspective on membrane compartment organization. *Nature,* 409**,** 839-841.

CATALANO, C. M., CZYMMEK, K. J., GANN, J. G. & SHERRIER, D. J. 2007. Medicago truncatula syntaxin SYP132 defines the symbiosome membrane and infection droplet membrane in root nodules. *Planta,* 225**,** 541-50.

CERTAL, A. C., ALMEIDA, N. F., CARVALHO, L. M., WONG, E., MORENO, N., MICHARD, E., CARNEIRO, J., RODRIGUEZ-LEON, J., WU, H. M., CHEUNG, A. Y. & FEIJO, J. A. 2008. Exclusion of a proton ATPase from the apical membrane is associated with cell polarity and tip growth in Nicotiana tabacum pollen tubes. *Plant Cell,* 20**,** 614-634.

CHITRAKAR, R. & MELOTTO, M. 2010. Assessing Stomatal Response to Live Bacterial Cells using Whole Leaf Imaging. *JoVE***,** e2185.

CLOUGH, S. J. & BENT, A. F. 1998. Floral dip: a simplified method for Agrobacterium-mediated transformation of Arabidopsis thaliana. *Plant Journal,* 16**,** 735-743.

COSGROVE, D. J. 1987. Wall relaxation and the driving forces for cell expansive growth. *Plant Physiology,* 84**,** 561-564.

DHONUKSHE, P., ANIENTO, F., HWANG, I., ROBINSON, D. G., MRAVEC, J., STIERHOF, Y. D. & FRIML, J. 2007. Clathrin-mediated constitutive endocytosis of PIN auxin efflux carriers in Arabidopsis *Current Biology,* 17**,** 520-527.

DI SANSEBASTIANO, G. P., BAROZZI, F., PIRO, G., DENECKE, J. & DE MARCOS LOUSA, C. 2017. Trafficking routes to the plant vacuole: connecting alternative and classical pathways. *J Exp Bot,* 69**,** 79-90.

EISENACH, C., CHEN, Z. H., GREFEN, C. & BLATT, M. R. 2012. The trafficking protein SYP121 of Arabidopsis connects programmed stomatal closure and K^+ channel acivity with vegetative growth. *Plant Journal,* 69**,** 241-251.

EISENACH, C., PAPANATSIOU, M., HILLERT, E. K. & BLATT, M. R. 2014. Clustering of the K^+ channel GORK of Arabidopsis parallels its gating by extracellular K^+ *Plant Journal,* 78**,** 203-214.

EL KASMI, F., KRAUSE, C., HILLER, U., STIERHOF, Y.-D., MAYER, U., CONNER, L., KONG, L., REICHARDT, I., SANDERFOOT, A. A. & JUERGENS, G. 2013. SNARE complexes of different composition jointly mediate membrane fusion in Arabidopsis cytokinesis. *Molecular Biology of the Cell,* 24**,** 1593-1601.

ENAMI, K., ICHIKAWA, M., UEMURA, T., KUTSUNA, N., HASEZAWA, S., NAKAGAWA, T., NAKANO, A. & SATO, M. H. 2009. Differential Expression Control and Polarized Distribution of Plasma

Membrane-Resident SYP1 SNAREs in Arabidopsis thaliana *Plant and Cell Physiology,* 50**,** 280-289.

EVANS, M. L., ISHIKAWA, H. & ESTELLE, M. A. 1994. Responses of Arabidopsis Roots to Auxin Studied with High Temporal Resolution - Comparison of Wild-Type and Auxin-Response Mutants. *Planta,* 194**,** 215-222.

FARACO, M., LI, Y., LI, S., SPELT, C., DI SANSEBASTIANO, G. P., REALE, L., FERRANTI, F., VERWEIJ, W., KOES, R. & QUATTROCCHIO, F. M. 2017. A Tonoplast P3B-ATPase Mediates Fusion of Two Types of Vacuoles in Petal Cells. *Cell Rep,* 19**,** 2413-2422.

FASSHAUER, D., ELIASON, W. K., BRUNGER, A. T. & JAHN, R. 1998. Identification of a minimal core of the synaptic SNARE complex sufficient for reversible assembly and disassembly. *Biochemistry,* 37**,** 10354-10362.

FENDRYCH, M., LEUNG, J. & FRIML, J. 2016. TIR1/AFB-Aux/IAA auxin perception mediates rapid cell wall acidification and growth of Arabidopsis hypocotyls. *Elife,* 5.

FORESTI, O., DASILVA, L. L. P. & DENECKE, J. 2006. Overexpression of the Arabidopsis syntaxin PEP12/SYP21 inhibits transport from the prevacuolar compartment to the lytic vacuole in vivo. *Plant Cell,* 18**,** 2275-2293.

FUGLSANG, A. T., BORCH, J., BYCH, K., JAHN, T. P., ROEPSTORFF, P. & PALMGREN, M. G. 2003. The binding site for regulatory 14-3-3 protein in plant plasma membrane H+-ATPase: involvement of a region promoting phosphorylation-independent interaction in addition to the phosphorylation-dependent C-terminal end. *J Biol Chem,* 278**,** 42266-72.

FUJIWARA, M., UEMURA, T., EBINE, K., NISHIMORI, Y., UEDA, T., NAKANO, A., SATO, M. H. & FUKAO, Y. 2014. Interactomics of Qa-SNARE in Arabidopsis thaliana. *Plant and Cell Physiology,* 55**,** 781-789.

GAFFIELD, M. A. & BETZ, W. J. 2006. Imaging synaptic vesicle exocytosis and endocytosis with FM dyes. *Nat Protoc,* 1**,** 2916-21.

GEELEN, D., LEYMAN, B., BATOKO, H., DI SANSEBASTIANO, G. P., MOORE, I. & BLATT, M. R. 2002. The abscisic acid-related SNARE homolog NtSyr1 contributes to secretion and growth: evidence from competition with its cytosolic domain. *Plant Cell,* 14**,** 387-406.

GELDNER, N., ANDERS, N., WOLTERS, H., KEICHER, J., KORNBERGER, W., MULLER, P., DELBARRE, A., UEDA, T., NAKANO, A. & JURGENS, G. 2003. The Arabidopsis GNOM ARF-GEF mediates endosomal recycling, auxin transport, and auxin-dependent plant growth. *Cell,* 112**,** 219-230.

GREFEN, C. & BLATT, M. R. 2012. A 2in1 cloning system enables ratiometric bimolecular fluorescence complementation (rBiFC). *Biotechniques,* 53**,** 311-314.

GREFEN, C., DONALD, N., HASHIMOTO, K., KUDLA, J., SCHUMACHER, K. & BLATT, M. R. 2010. A ubiquitin-10 promoter-based vector set for fluorescent protein tagging facilitates temporal stability and native protein distribution in transient and stable expression studies. *Plant Journal,* 64**,** 355-365.

GREFEN, C., KARNIK, R., LARSON, E., LEFOULON, C., WANG, Y., WAGHMARE, S., ZHANG, B., HILLS, A. & BLATT, M. R. 2015. A vesicle-trafficking protein commandeers Kv channel voltage sensors for voltage-dependent secretion. *Nat Plants,* 1**,** 15108.

HAGER, A. 2003. Role of the plasma membrane H+-ATPase in auxin-induced elongation growth: historical and new aspects. *J Plant Res,* 116**,** 483-505.

HAGER, A., DEBUS, G., EDEL, H. G., STRANSKY, H. & SERRANO, R. 1991. Auxin induces exocytosis and the rapid synthesis of a high-turnover pool of plasma-membrane H(+)-ATPase. *Planta,* 185**,** 527-37.

HAGER, A., MENZEL, H. & KRAUSS, A. 1971. [Experiments and hypothesis concerning the primary action of auxin in elongation growth]. *Planta,* 100**,** 47-75.

HARPER, J. F., SUROWY, T. K. & SUSSMAN, M. R. 1989. Molecular cloning and sequence of cDNA encoding the plasma membrane proton pump (H + -ATPase) of Arabidopsis thaliana *Proceedings Of The National Academy Of Sciences Of The United States Of America,* 86**,** 1234-1238.

1226 HARRISON, S. J., MOTT, E. K., PARSLEY, K., ASPINALL, S., GRAY, J. C. & COTTAGE, A. 2006. A rapid and
1227 robust method of identifying transformed Arabidopsis thaliana seedlings following floral dip
1228 transformation. *Plant Methods,* 2**,** 19.
1229 HARUTA, M., BURCH, H. L., NELSON, R. B., BARRETT-WILT, G., KLINE, K. G., MOHSIN, S. B., YOUNG, J.
1230 C., OTEGUI, M. S. & SUSSMAN, M. R. 2010. Molecular characterization of mutant Arabidopsis
1231 plants with reduced plasma membrane proton pump activity. *J Biol Chem,* 285**,** 17918-29.
1232 HARUTA, M., GRAY, W. M. & SUSSMAN, M. R. 2015. Regulation of the plasma membrane proton
1233 pump (H+-ATPase) by phosphorylation. *Current Opinion in Plant Biology,* 28**,** 68-75.
1234 HARUTA, M. & SUSSMAN, M. R. 2012. The effect of a genetically reduced plasma membrane
1235 protonmotive force on vegetative growth of Arabidopsis thaliana *Plant Physiology,*
1236 doi:10.1104/pp.111.189167.
1237 HASHIMOTO-SUGIMOTO, M., HIGAKI, T., YAENO, T., NAGAMI, A., IRIE, M., FUJIMI, M., MIYAMOTO,
1238 M., AKITA, K., NEGI, J., SHIRASU, K., HASEZAWA, S. & IBA, K. 2013. A Munc13-like protein in
1239 Arabidopsis mediates H^+-ATPase translocation that is essential for stomatal responses.
1240 *Nature Communications,* 4.
1241 HEARD, W., SKLENÁŘ, J., TOMÉ, D. F. A., ROBATZEK, S. & JONES, A. M. E. 2015. Identification of
1242 Regulatory and Cargo Proteins of Endosomal and Secretory Pathways in Arabidopsis thaliana
1243 by Proteomic Dissection. *Molecular & Cellular Proteomics : MCP,* 14**,** 1796-1813.
1244 HECKER, A., WALLMEROTH, N, PETER, S, BLATT, MR, HARTER, K, GREFEN, C 2015. Binary 2in1 vectors
1245 improve in planta (co-) localisation and dynamic protein interaction studies. *Plant*
1246 *Physiology,* 168**,** 776-87.
1247 HIGAKI, T., HASHIMOTO-SUGIMOTO, M., AKITA, K., IBA, K. & HASEZAWA, S. 2014. Dynamics and
1248 environmental responses of PATROL1 in Arabidopsis subsidiary cells. *Plant Cell Physiol,* 55**,**
1249 773-80.
1250 HONSBEIN, A., SOKOLOVSKI, S., GREFEN, C., CAMPANONI, P., PRATELLI, R., PANEQUE, M., CHEN, Z.,
1251 JOHANSSON, I. & BLATT, M. R. 2009. A tripartite SNARE-K+ channel complex mediates in
1252 channel-dependent K+ nutrition in Arabidopsis. *Plant Cell,* 21**,** 2859-77.
1253 HUISMAN, R., HONTELEZ, J., MYSORE, K. S., WEN, J., BISSELING, T. & LIMPENS, E. 2016. A symbiosis-
1254 dedicated SYNTAXIN OF PLANTS 13II isoform controls the formation of a stable host-microbe
1255 interface in symbiosis. *New Phytol,* 211**,** 1338-51.
1256 ICHIKAWA, M., HIRANO, T., ENAMI, K., FUSELIER, T., KATO, N., KWON, C., VOIGT, B., SCHULZE-
1257 LEFERT, P., BALUSKA, F. & SATO, M. H. 2014. Syntaxin of plant proteins SYP123 and SYP132
1258 mediate root hair tip growth in Arabidopsis thaliana. *Plant Cell Physiol,* 55**,** 790-800.
1259 JAHN, R. & SCHELLER, R. H. 2006. SNAREs - engines for membrane fusion. *Nature Reviews Molecular*
1260 *Cell Biology,* 7**,** 631-643.
1261 JEZEK, M. & BLATT, M. R. 2017. The Membrane Transport System of the Guard Cell and Its
1262 Integration for Stomatal Dynamics. *Plant Physiol,* 174**,** 487-519.
1263 KALDE, M., NUHSE, T. S., FINDLAY, K. & PECK, S. C. 2007. The syntaxin SYP132 contributes to plant
1264 resistance against bacteria and secretion of pathogenesis-related protein 1. *Proceedings Of*
1265 *The National Academy Of Sciences Of The United States Of America,* 104**,** 11850-11855.
1266 KARGUL, J., GANSEL, X., TYRRELL, M., STICHER, L. & BLATT, M. R. 2001. Protein-binding partners of
1267 the tobacco syntaxin NtSyr1. *FEBS Letters,* 508**,** 253-258.
1268 KARIMI, M., INZE, D. & DEPICKER, A. 2002. GATEWAY vectors for Agrobacterium -mediated plant
1269 transformation. *Trends In Plant Science,* 7**,** 193-195.
1270 KARNAHL, M., PARK, M., KRAUSE, C., HILLER, U., MAYER, U., STIERHOF, Y. D. & JURGENS, G. 2018.
1271 Functional diversification of Arabidopsis SEC1-related SM proteins in cytokinetic and
1272 secretory membrane fusion. *Proc Natl Acad Sci U S A,* 115**,** 6309-6314.
1273 KARNIK, R., GREFEN, C., BAYNE, R., HONSBEIN, A., KOHLER, T., KIOUMOURTZOGLOU, D., WILLIAMS,
1274 M., BRYANT, N. J. & BLATT, M. R. 2013. Arabidopsis Sec1/Munc18 protein SEC11 is a
1275 competitive and dynamic modulator of SNARE binding and SYP121-dependent vesicle traffic.
1276 *Plant Cell,* 25**,** 1368-82.

KARNIK, R., WAGHMARE, S., ZHANG, B., LARSON, E., LEFOULON, C., GONZALEZ, W. & BLATT, M. R. 2017. Commandeering Channel Voltage Sensors for Secretion, Cell Turgor, and Volume Control. *Trends Plant Sci,* 22**,** 81-95.

KARNIK, R., ZHANG, B., WAGHMARE, S., ADERHOLD, C., GREFEN, C. & BLATT, M. R. 2015. Binding of SEC11 indicates its role in SNARE recycling after vesicle fusion and identifies two pathways for vesicular traffic to the plasma membrane. *Plant Cell,* 27**,** 675-94.

KAUNDAL, A., RAMU, V. S., OH, S., LEE, S., PANT, B., LEE, H. K., ROJAS, C. M., SENTHIL-KUMAR, M. & MYSORE, K. S. 2017. GENERAL CONTROL NONREPRESSIBLE4 Degrades 14-3-3 and the RIN4 Complex to Regulate Stomatal Aperture with Implications on Nonhost Disease Resistance and Drought Tolerance. *Plant Cell,* 29**,** 2233-2248.

KINOSHITA, T. & SHIMAZAKI, K. 1999. Blue light activates the plasma membrane H^+ -ATPase by phosphorylation of the C-terminus in stomatal guard cells. *EMBO Journal,* 18**,** 5548-5558.

KITAKURA, S., VANNESTE, S., ROBERT, S., LOFKE, C., TEICHMANN, T., TANAKA, H. & FRIML, J. 2011. Clathrin mediates endocytosis and polar distribution of PIN auxin transporters in Arabidopsis. *Plant Cell,* 23**,** 1920-31.

LARSON, E. R., VAN ZELM, E., ROUX, C., MARION-POLL, A. & BLATT, M. R. 2017. Clathrin Heavy Chain Subunits Coordinate Endo- and Exocytic Traffic and Affect Stomatal Movement. *Plant Physiol,* 175**,** 708-720.

LEE, M. H., MIN, M. K., LEE, Y. J., JIN, J. B., SHIN, D. H., KIM, D. H., LEE, K. H. & HWANG, I. 2002. ADP-ribosylation factor 1 of Arabidopsis plays a critical role in intracellular trafficking and maintenance of endoplasmic reticulum morphology in Arabidopsis. *Plant Physiol,* 129**,** 1507-20.

LIMPENS, E., IVANOV, S., VAN ESSE, W., VOETS, G., FEDOROVA, E. & BISSELING, T. 2009. Medicago N2-fixing symbiosomes acquire the endocytic identity marker Rab7 but delay the acquisition of vacuolar identity. *Plant Cell,* 21**,** 2811-28.

LIVAK, K. J. & SCHMITTGEN, T. D. 2001. Analysis of relative gene expression data using real-time quantitative PCR and the 2(-Delta Delta C(T)) Method. *Methods,* 25**,** 402-8.

MACROBBIE, E. A. C. 1991. Effect of ABA on ion transport and stomatal regulation. *In:* DAVIES, W. J. & JONES, H. G. (eds.) *Abscisic Acid Physiology and Biochemistry.* Oxford: Bios Scientific.

MARRE, E. 1979. FUSICOCCIN - TOOL IN PLANT PHYSIOLOGY. *Annual Review of Plant Physiology and Plant Molecular Biology,* 30**,** 273-288.

MARWAHA, R. & SHARMA, M. 2017. DQ-Red BSA Trafficking Assay in Cultured Cells to Assess Cargo Delivery to Lysosomes. *Bio Protoc,* 7.

MECKEL, T., HURST, A. C., THIEL, G. & HOMANN, U. 2004. Endocytosis against high turgor: intact guard cells of Vicia faba constitutively endocytose fluorescently labelled plasma membrane and GFP-tagged K-channel KAT1. *Plant J,* 39**,** 182-93.

MERLOT, S., LEONHARDT, N., FENZI, F., VALON, C., COSTA, M., PIETTE, L., VAVASSEUR, A., GENTY, B., BOIVIN, K., MULLER, A., GIRAUDAT, J. & LEUNG, J. 2007. Constitutive activation of a plasma membrane H(+)-ATPase prevents abscisic acid-mediated stomatal closure. *EMBO J,* 26**,** 3216-26.

MICHELET, B. & BOUTRY, M. 1995. The Plasma Membrane H+-ATPase (A Highly Regulated Enzyme with Multiple Physiological Functions). *Plant Physiol,* 108**,** 1-6.

OMELYANCHUK, N. A., WIEBE, D. S., NOVIKOVA, D. D., LEVITSKY, V. G., KLIMOVA, N., GORELOVA, V., WEINHOLDT, C., VASILIEV, G. V., ZEMLYANSKAYA, E. V., KOLCHANOV, N. A., KOCHETOV, A. V., GROSSE, I. & MIRONOVA, V. V. 2017. Auxin regulates functional gene groups in a fold-change-specific manner in Arabidopsis thaliana roots. *Sci Rep,* 7**,** 2489.

PALMGREN, M. G. 2001. Plant plasma membrane H^+ -ATPases: Powerhouses for nutrient uptake. *Annual Review Of Plant Physiology And Plant Molecular Biology,* 52**,** 817-845.

PALMGREN, M. G., BAEKGAARD, L., LOPEZ-MARQUES, R. L. & FUGLSANG, A. T. 2011. Plasma Membrane ATPases. *In:* MURPHY, A., PEER, W. A. & SCHULZ, B. (eds.) *Plant Plasma Membrane.*

PAN, H., OZTAS, O., ZHANG, X., WU, X., STONOHA, C., WANG, E., WANG, B. & WANG, D. 2016. A symbiotic SNARE protein generated by alternative termination of transcription. *Nat Plants,* 2**,** 15197.

PARK, M., KRAUSE, C., KARNAHL, M., REICHARDT, I., EL KASMI, F., MAYER, U., STIERHOF, Y. D., HILLER, U., STROMPEN, G., BAYER, M., KIENTZ, M., SATO, M. H., NISHIMURA, M. T., DANGL, J. L., SANDERFOOT, A. A. & JURGENS, G. 2018. Concerted Action of Evolutionarily Ancient and Novel SNARE Complexes in Flowering-Plant Cytokinesis. *Dev Cell,* 44**,** 500-511 e4.

RAFIQI, M., GAN, P. H. P., RAVENSDALE, M., LAWRENCE, G. J., ELLIS, J. G., JONES, D. A., HARDHAM, A. R. & DODDS, P. N. 2010. Internalization of Flax Rust Avirulence Proteins into Flax and Tobacco Cells Can Occur in the Absence of the Pathogen. *Plant Cell,* 22**,** 2017-2032.

RAYLE, D. L. & CLELAND, R. 1970. Enhancement of wall loosening and elongation by Acid solutions. *Plant Physiol,* 46**,** 250-3.

ROELFSEMA, M. R. G. & HEDRICH, R. 2005. In the light of stomatal opening: new insights into 'the Watergate'. *New Phytologist,* 167**,** 665-691.

SANDERFOOT, A. 2007. Increases in the number of SNARE genes parallels the rise of multicellularity among the green plants. *Plant Physiology,* 144**,** 6-17.

SAPONARO, A., PORRO, A., CHAVES-SANJUAN, A., NARDINI, M., RAUH, O., THIEL, G. & MORONI, A. 2017. Fusicoccin Activates KAT1 Channels by Stabilizing Their Interaction with 14-3-3 Proteins. *Plant Cell,* 29**,** 2570-2580.

SCHINDELIN, J., ARGANDA-CARRERAS, I., FRISE, E., KAYNIG, V., LONGAIR, M., PIETZSCH, T., PREIBISCH, S., RUEDEN, C., SAALFELD, S., SCHMID, B., TINEVEZ, J.-Y., WHITE, D. J., HARTENSTEIN, V., ELICEIRI, K., TOMANCAK, P. & CARDONA, A. 2012. Fiji: an open-source platform for biological-image analysis. *Nature Methods,* 9**,** 676.

SCHINDLER, T., BERGFELD, R., HOHL, M. & SCHOPFER, P. 1994. Inhibition of golgi apparatus function by brefeldin A in maize coleoptiles and its consequences on auxin-mediated growth, cell-wall extensibility and secretion of cell wall proteins. *Planta,* 192**,** 404-413.

SHIMAZAKI, K. I., DOI, M., ASSMANN, S. M. & KINOSHITA, T. 2007. Light regulation of stomatal movement. *Annual Review of Plant Biology,* 58**,** 219-247.

SHOPE, J. C., PEAK, D. & MOTT, K. A. 2008. Stomatal responses to humidity in isolated epidermes. *Plant Cell And Environment,* 31**,** 1290-1298.

SKLODOWSKI, K., RIEDELSBERGER, J., RADDATZ, N., RIADI, G., CABALLERO, J., CHEREL, I., SCHULZE, W., GRAF, A. & DREYER, I. 2017. The receptor-like pseudokinase MRH1 interacts with the voltage-gated potassium channel AKT2. *Sci Rep,* 7**,** 44611.

SONDERGAARD, T. E., SCHULZ, A. & PALMGREN, M. G. 2004. Energization of transport processes in plants. roles of the plasma membrane H+-ATPase. *Plant Physiol,* 136**,** 2475-82.

SUDHOF, T. C. & ROTHMAN, J. E. 2009. Membrane Fusion: Grappling with SNARE and SM Proteins. *Science,* 323**,** 474-477.

SUTTER, J. U., CAMPANONI, P., TYRRELL, M. & BLATT, M. R. 2006. Selective mobility and sensitivity to SNAREs is exhibited by the Arabidopsis KAT1 K^+ channel at the plasma membrane. *Plant Cell,* 18**,** 935-954.

SUTTER, J. U., SIEBEN, C., HARTEL, A., EISENACH, C., THIEL, G. & BLATT, M. R. 2007. Abscisic acid triggers the endocytosis of the Arabidopsis KAT1 K^+ channel and its recycling to the plasma membrane. *Current Biology,* 17**,** 1396-1402.

SZE, H., LI, X. H. & PALMGREN, M. G. 1999. Energization of plant cell membranes by H^+ -pumping ATPases: Regulation and biosynthesis. *Plant Cell,* 11**,** 677-689.

THIEL, G., BLATT, M. R., FRICKER, M. D., WHITE, I. R. & MILLNER, P. 1993. Modulation of K+ channels in Vicia stomatal guard cells by peptide homologs to the auxin-binding protein C terminus. *Proc Natl Acad Sci U S A,* 90**,** 11493-7.

TYRRELL, M., CAMPANONI, P., SUTTER, J. U., PRATELLI, R., PANEQUE, M., SOKOLOVSKI, S. & BLATT, M. R. 2007. Selective targeting of plasma membrane and tonoplast traffic by inhibitory (dominant-negative) SNARE fragments. *Plant J,* 51**,** 1099-115.

VELASQUEZ, S. M., BARBEZ, E., KLEINE-VEHN, J. & ESTEVEZ, J. M. 2016. Auxin and Cellular Elongation. *Plant Physiology,* 170**,** 1206-1215.

VIALET-CHABRAND, S., HILLS, A., WANG, Y., GRIFFITHS, H., LEW, V. L., LAWSON, T., BLATT, M. R. & ROGERS, S. 2017. Global Sensitivity Analysis of OnGuard Models Identifies Key Hubs for Transport Interaction in Stomatal Dynamics. *Plant Physiol,* 174**,** 680-688.

WAGHMARE, S., LILEIKYTE, E., KARNIK, R., GOODMAN, J. K., BLATT, M. R. & JONES, A. M. E. 2018. SNAREs SYP121 and SYP122 Mediate the Secretion of Distinct Cargo Subsets. *Plant Physiol,* 178**,** 1679-1688.

WANG, Y., NOGUCHI, K., ONO, N., INOUE, S. I., TERASHIMA, I. & KINOSHITA, T. 2014. Overexpression of plasma membrane H^+ -ATPase in guard cells promotes light-induced stomatal opening and enhances plant growth. *Proc.Nat.Acad.Sci.USA,* 111**,** 533-538.

XUE, Y., YANG, Y., YANG, Z., WANG, X. & GUO, Y. 2018. VAMP711 Is Required for Abscisic Acid-Mediated Inhibition of Plasma Membrane H(+)-ATPase Activity. *Plant Physiol,* 178**,** 1332-1343.

YAMAUCHI, S., TAKEMIYA, A., SAKAMOTO, T., KURATA, T., TSUTSUMI, T., KINOSHITA, T. & SHIMAZAKI, K.-I. 2016. The Plasma Membrane H^+-ATPase AHA1 Plays a Major Role in Stomatal Opening in Response to Blue Light. *Plant Physiology,* 171**,** 2731-2743.

YANG, H. & MURPHY, A. 2013. Membrane Preparation, Sucrose Density Gradients and Two-phase Separation Fractionation from Five-day-old Arabidopsis seedlings. *The Plant Journal*.

YOSHIDA, S., UEMURA, M., NIKI, T., SAKAI, A. & GUSTA, L. V. 1983. Partition of membrane particles in aqueous two-polymer phase system and its practical use for purification of plasma membranes from plants. *Plant Physiol,* 72**,** 105-14.

ZHANG, B., KARNIK, R., DONALD, N. & BLATT, M. R. 2018. A GPI Signal Peptide-Anchored Split-Ubiquitin (GPS) System for Detecting Soluble Bait Protein Interactions at the Membrane. *Plant Physiol,* 178**,** 13-17.

ZHANG, B., KARNIK, R., WANG, Y., WALLMEROTH, N., BLATT, M. R. & GREFEN, C. 2015. The Arabidopsis R-SNARE VAMP721 Interacts with KAT1 and KC1 K^+ Channels to Moderate K^+ Current at the Plasma Membrane. *Plant Cell,* 27**,** 1697-717.

ZHANG, X., WANG, H. B., TAKEMIYA, A., SONG, C. P., KINOSHITA, T. & SHIMAZAKI, K. I. 2004. Inhibition of blue light-dependent H^+ pumping by abscisic acid through hydrogen peroxide-induced dephosphorylation of the plasma membrane H^+ -ATPase in guard cell protoplasts. *Plant Physiology,* 136**,** 4150-4158.

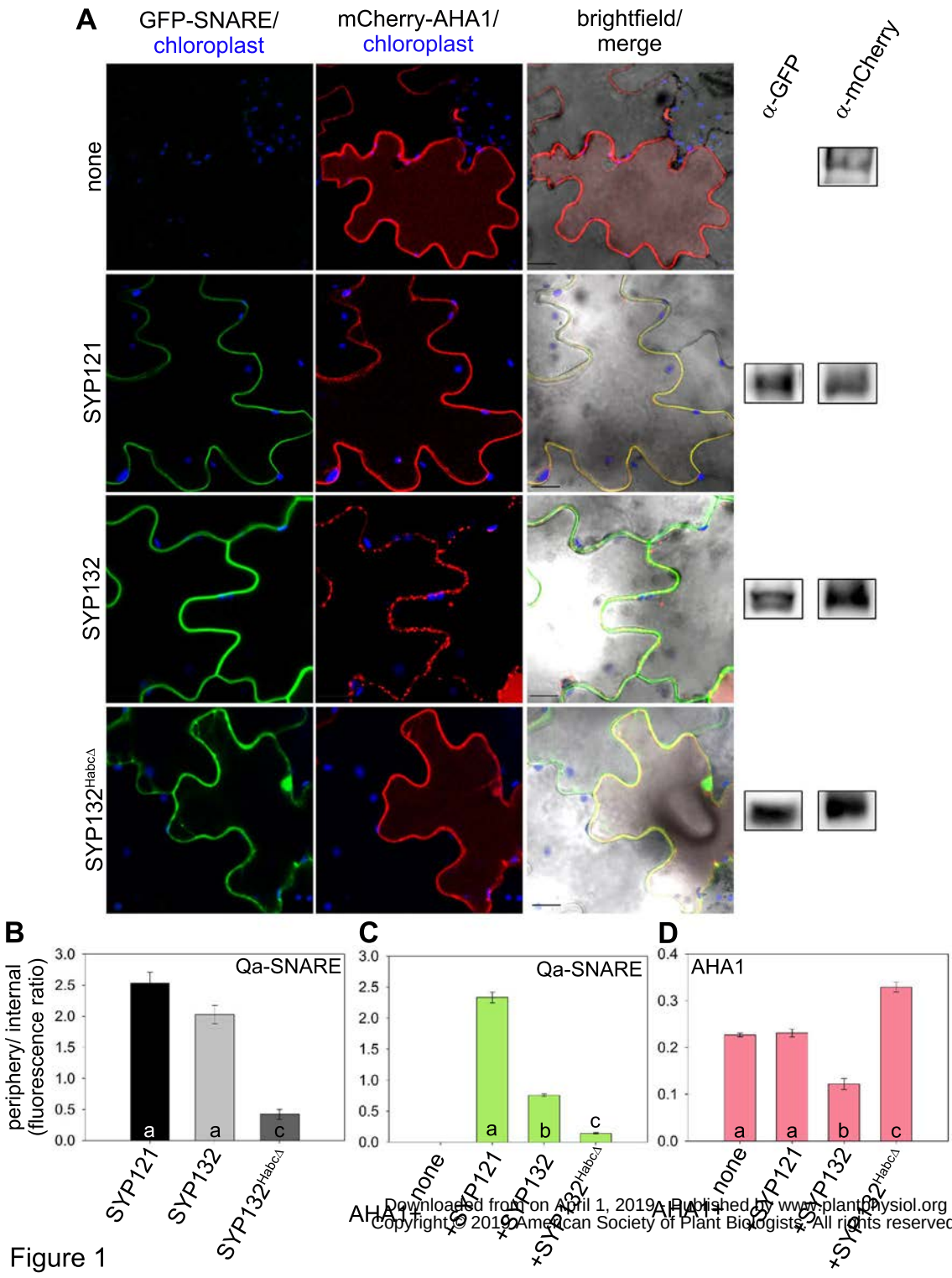

Figure 1

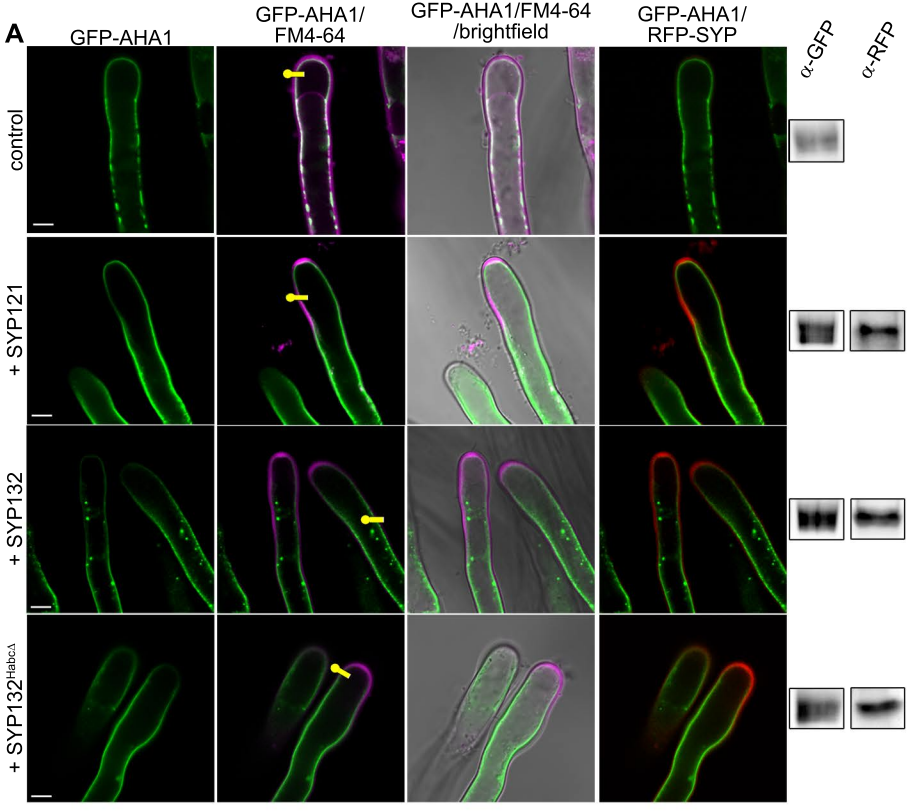

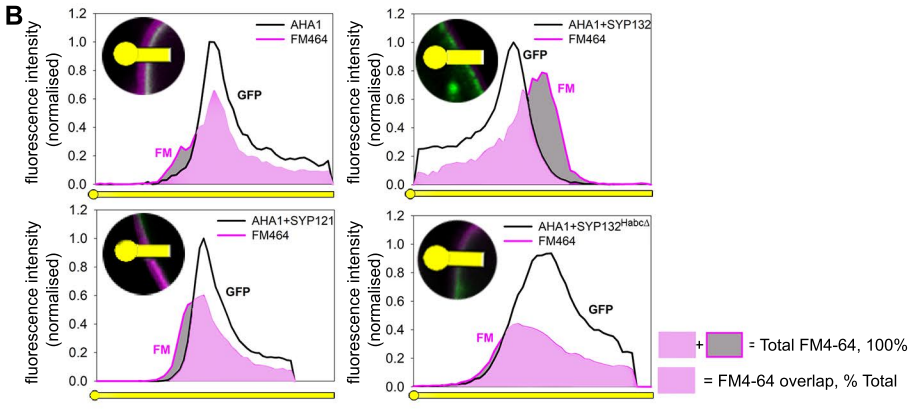

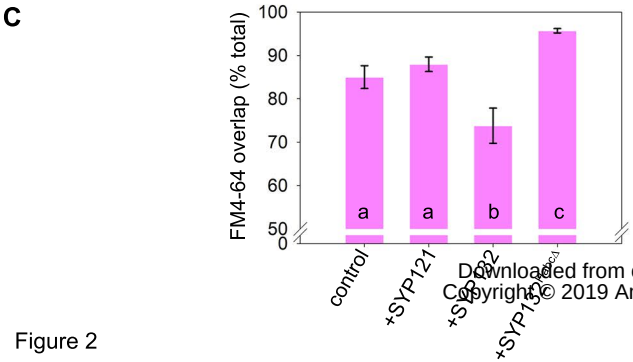

Figure 2

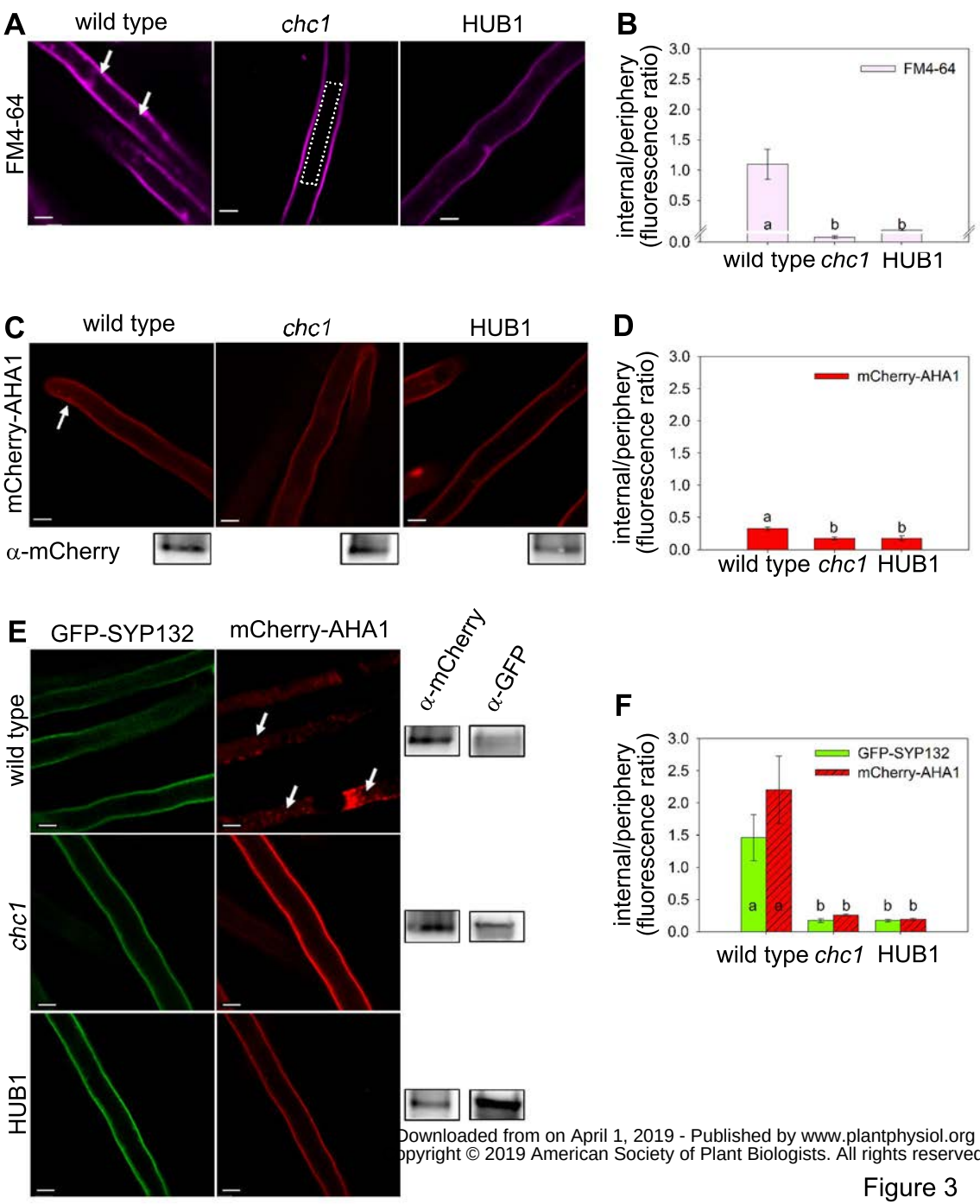

Figure 3

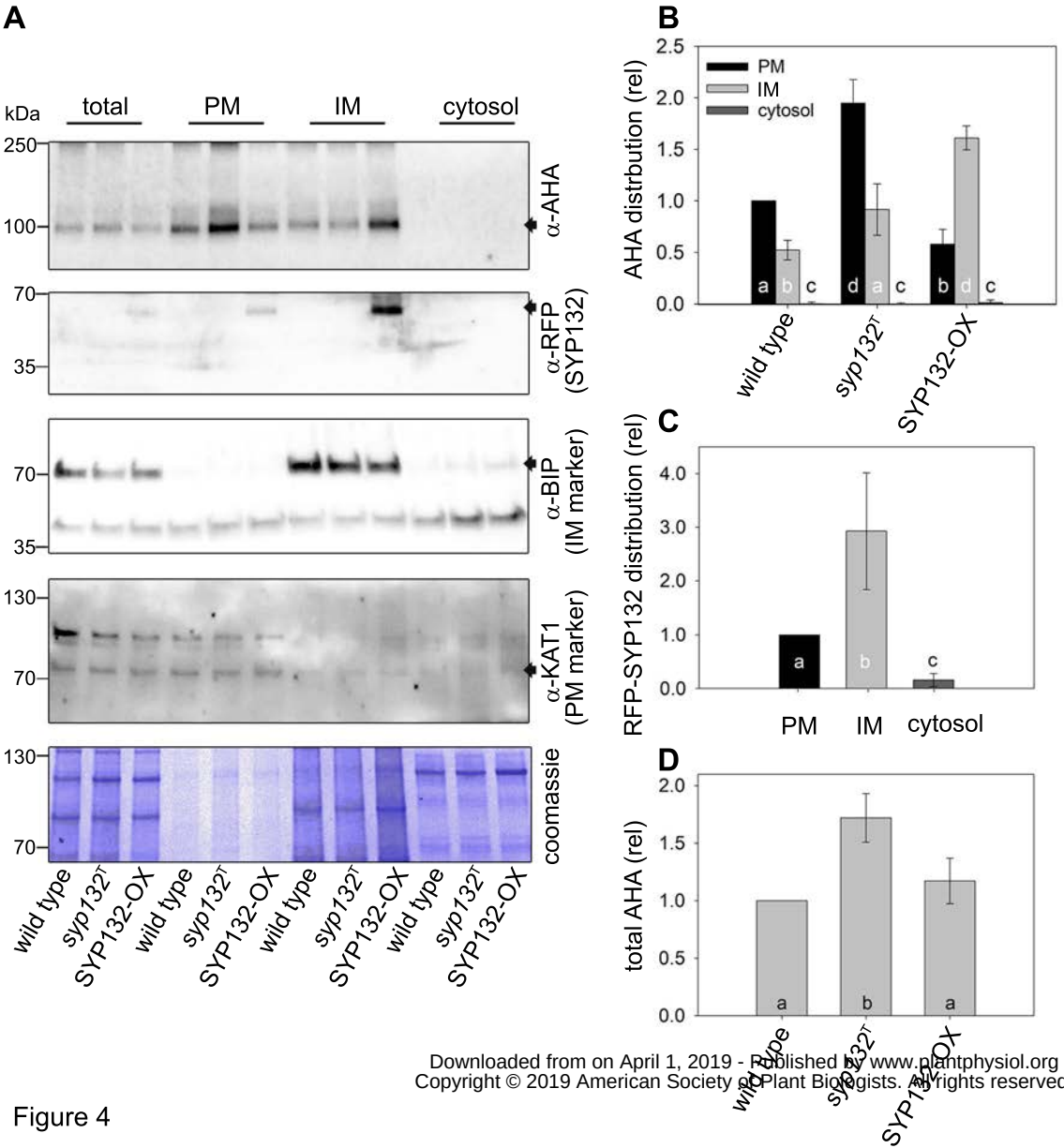

Figure 4

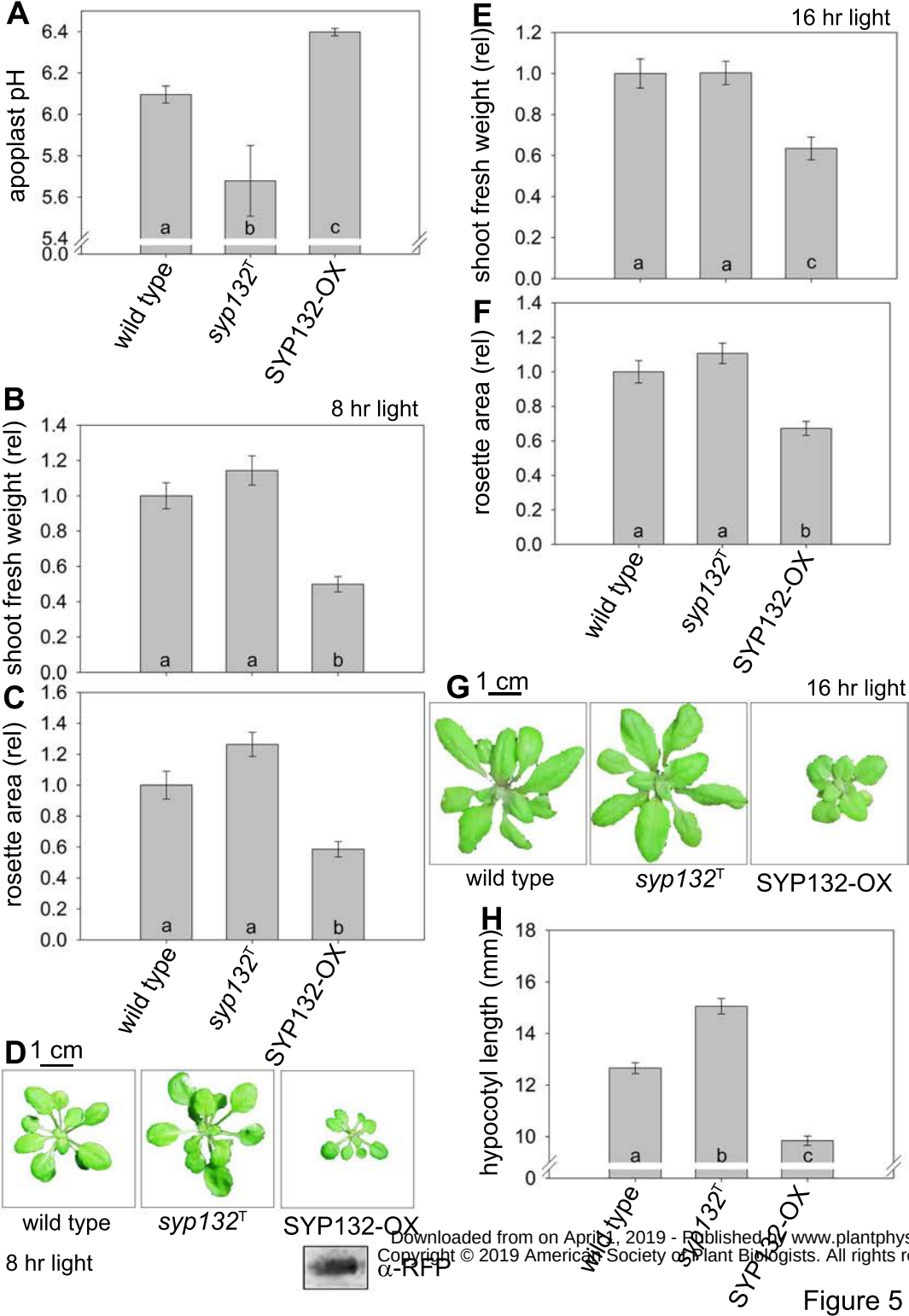

Figure 5

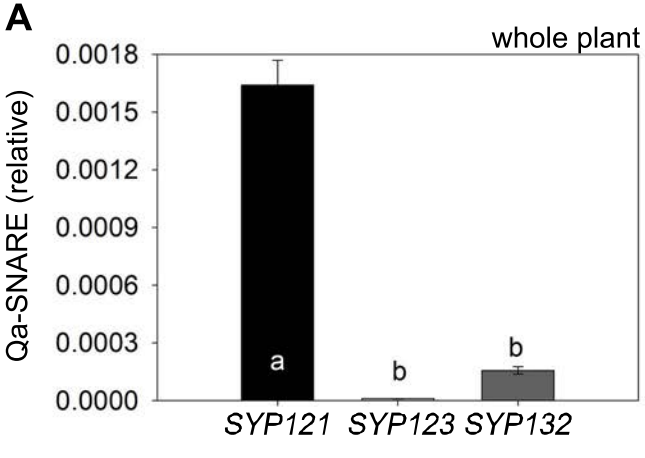

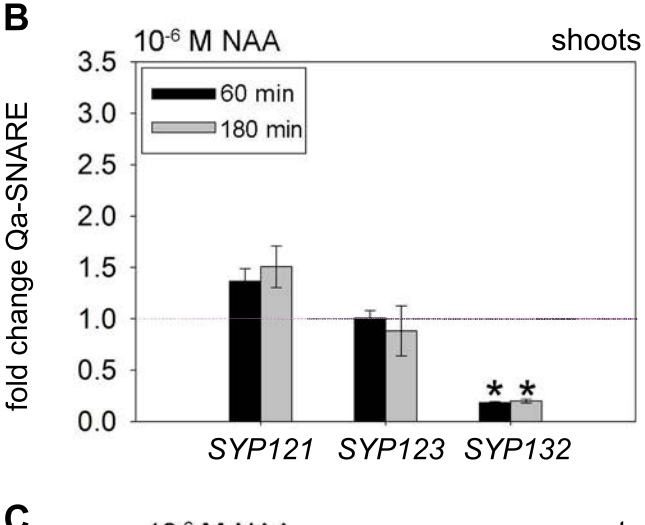

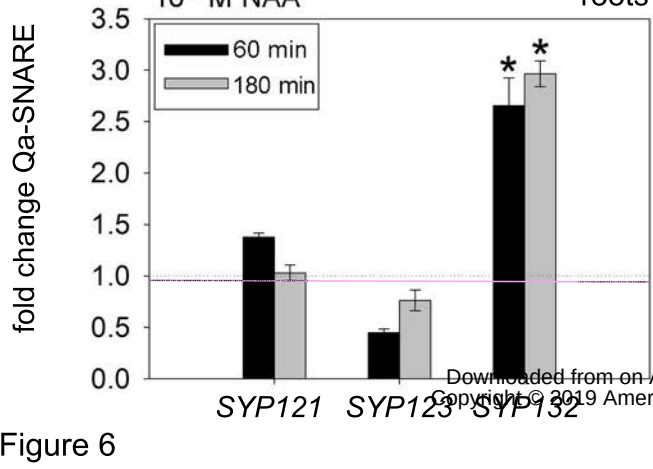

Figure 6

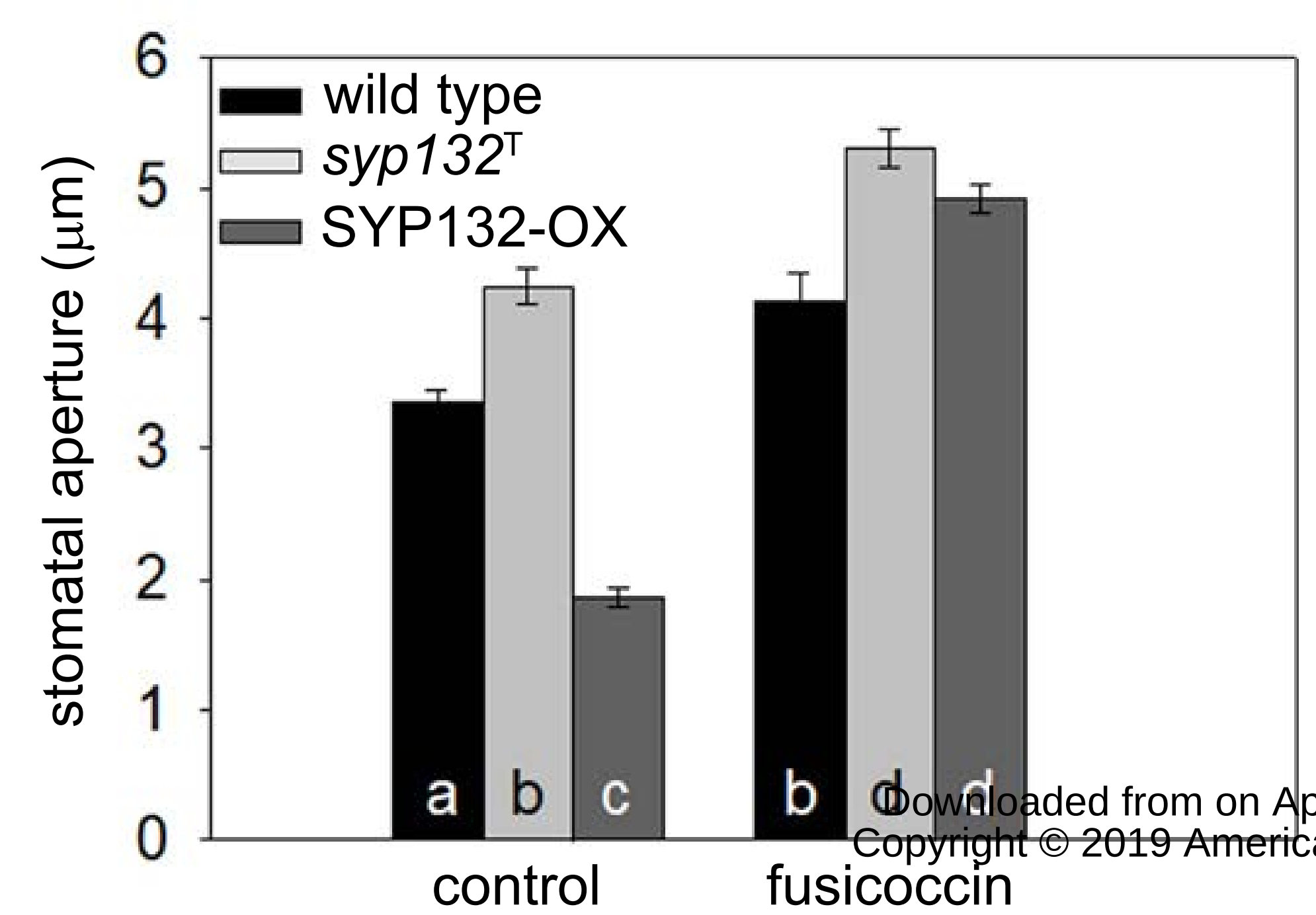

Figure 7

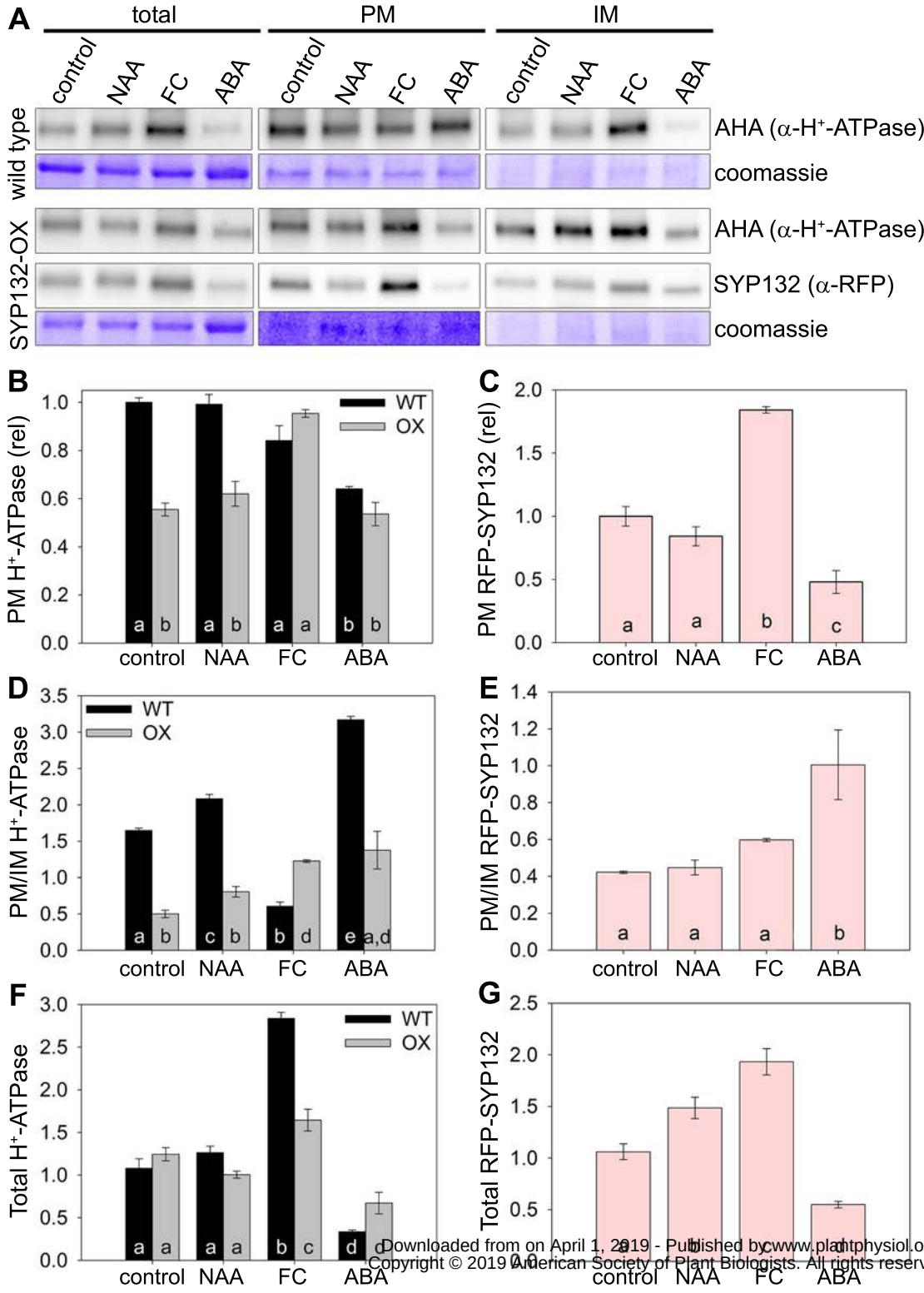

Figure 8

Figure 9

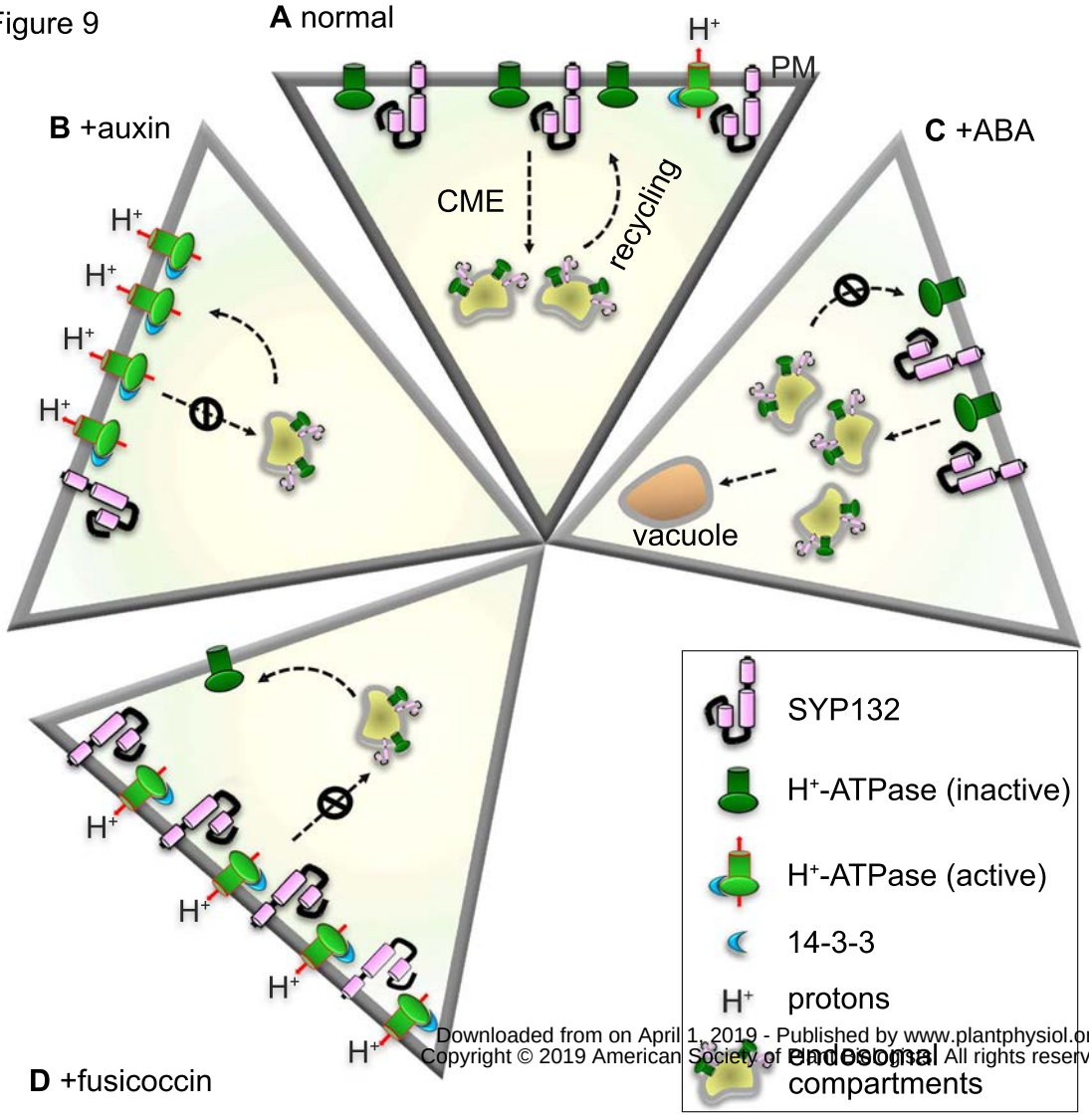

Parsed Citations

ADVANI, R. J., YANG, B., PREKERIS, R., LEE, K. C., KLUMPERMAN, J. & SCHELLER, R. H. 1999. VAMP-7 mediates vesicular transport from endosomes to lysosomes. Journal Of Cell Biology, 146, 765-775.

Pubmed: Author and Title
Google Scholar: Author Only Title Only Author and Title

ALEXANDERSSON, E., GUSTAVSSON, N., BERNFUR, K., KARLSSON, A., KJELLBOM, P. & LARSSON, C. 2008. Purification and proteomic analysis of plant plasma membranes. Methods Mol Biol, 432, 161-73.

Pubmed: Author and Title
Google Scholar: Author Only Title Only Author and Title

ARANGO, M., GEVAUDANT, F., OUFATTOLE, M. & BOUTRY, M. 2003. The plasma membrane proton pump ATPase: the significance of gene subfamilies. Planta, 216, 355-65.

Pubmed: Author and Title
Google Scholar: Author Only Title Only Author and Title

ASSAAD, F. F., QIU, J. L., YOUNGS, H., EHRHARDT, D., ZIMMERLI, L., KALDE, M., WANNER, G., PECK, S. C., EDWARDS, H., RAMONELL, K., SOMERVILLE, C. R. & THORDAL-CHRISTENSEN, H. 2004. The PEN1 syntaxin defines a novel cellular compartment upon fungal attack and is required for the timely assembly of papillae. Molecular Biology Of The Cell, 15, 5118-5129.

Pubmed: Author and Title
Google Scholar: Author Only Title Only Author and Title

BAROZZI, F., PAPADIA, P., STEFANO, G., RENNA, L., BRANDIZZI, F., MIGONI, D., FANIZZI, F. P., PIRO, G. & DI SANSEBASTIANO, G. P. 2018. Variation in Membrane Trafficking Linked to SNARE AtSYP51 Interaction With Aquaporin NIP1;1. Front Plant Sci, 9, 1949.

Pubmed: Author and Title
Google Scholar: Author Only Title Only Author and Title

BASSHAM, D. C. & BLATT, M. R. 2008. SNAREs: Cogs and Coordinators in Signaling and Development. Plant Physiology, 147, 1504-1515.

Pubmed: Author and Title
Google Scholar: Author Only Title Only Author and Title

BOCK, J. B., MATERN, H. T., PEDEN, A. A. & SCHELLER, R. H. 2001. A genomic perspective on membrane compartment organization. Nature, 409, 839-841.

Pubmed: Author and Title
Google Scholar: Author Only Title Only Author and Title

CATALANO, C. M., CZYMMEK, K. J., GANN, J. G. & SHERRIER, D. J. 2007. Medicago truncatula syntaxin SYP132 defines the symbiosome membrane and infection droplet membrane in root nodules. Planta, 225, 541-50.

Pubmed: Author and Title
Google Scholar: Author Only Title Only Author and Title

CERTAL, A. C., ALMEIDA, N. F., CARVALHO, L. M., WONG, E., MORENO, N., MICHARD, E., CARNEIRO, J., RODRIGUEZ-LEON, J., WU, H. M., CHEUNG, A. Y. & FEIJO, J. A. 2008. Exclusion of a proton ATPase from the apical membrane is associated with cell polarity and tip growth in Nicotiana tabacum pollen tubes. Plant Cell, 20, 614-634.

Pubmed: Author and Title
Google Scholar: Author Only Title Only Author and Title

CHITRAKAR, R. & MELOTTO, M. 2010. Assessing Stomatal Response to Live Bacterial Cells using Whole Leaf Imaging. JoVE, e2185.

Pubmed: Author and Title
Google Scholar: Author Only Title Only Author and Title

CLOUGH, S. J. & BENT, A. F. 1998. Floral dip: a simplified method for Agrobacterium-mediated transformation of Arabidopsis thaliana. Plant Journal, 16, 735-743.

Pubmed: Author and Title
Google Scholar: Author Only Title Only Author and Title

COSGROVE, D. J. 1987. Wall relaxation and the driving forces for cell expansive growth. Plant Physiology, 84, 561-564.

Pubmed: Author and Title
Google Scholar: Author Only Title Only Author and Title

DHONUKSHE, P., ANIENTO, F., HWANG, I., ROBINSON, D. G., MRAVEC, J., STIERHOF, Y. D. & FRIML, J. 2007. Clathrin-mediated constitutive endocytosis of PIN auxin efflux carriers in Arabidopsis Current Biology, 17, 520-527.

Pubmed: Author and Title
Google Scholar: Author Only Title Only Author and Title

DI SANSEBASTIANO, G. P., BAROZZI, F., PIRO, G., DENECKE, J. & DE MARCOS LOUSA, C. 2017. Trafficking routes to the plant vacuole: connecting alternative and classical pathways. J Exp Bot, 69, 79-90.

Pubmed: Author and Title
Google Scholar: Author Only Title Only Author and Title

EISENACH, C., CHEN, Z. H., GREFEN, C. & BLATT, M. R. 2012. The trafficking protein SYP121 of Arabidopsis connects programmed stomatal closure and K+ channel activity with vegetative growth. Plant Journal, 69, 241-251.

Pubmed: Author and Title
Google Scholar: Author Only Title Only Author and Title

EISENACH, C., PAPANATSIOU, M., HILLERT, E. K. & BLATT, M. R. 2014. Clustering of the K+ channel GORK of Arabidopsis parallels its gating by extracellular K+ Plant Journal, 78, 203-214.
Pubmed: Author and Title
Google Scholar: Author Only Title Only Author and Title

EL KASMI, F., KRAUSE, C., HILLER, U., STIERHOF, Y.-D., MAYER, U., CONNER, L., KONG, L., REICHARDT, I., SANDERFOOT, A. A. & JUERGENS, G. 2013. SNARE complexes of different composition jointly mediate membrane fusion in Arabidopsis cytokinesis. Molecular Biology of the Cell, 24, 1593-1601.
Pubmed: Author and Title
Google Scholar: Author Only Title Only Author and Title

ENAMI, K., ICHIKAWA, M., UEMURA, T., KUTSUNA, N., HASEZAWA, S., NAKAGAWA, T., NAKANO, A. & SATO, M. H. 2009. Differential Expression Control and Polarized Distribution of Plasma Membrane-Resident SYP1 SNAREs in Arabidopsis thaliana Plant and Cell Physiology, 50, 280-289.
Pubmed: Author and Title
Google Scholar: Author Only Title Only Author and Title

EVANS, M. L., ISHIKAWA, H. & ESTELLE, M. A. 1994. Responses of Arabidopsis Roots to Auxin Studied with High Temporal Resolution - Comparison of Wild-Type and Auxin-Response Mutants. Planta, 194, 215-222.
Pubmed: Author and Title
Google Scholar: Author Only Title Only Author and Title

FARACO, M., LI, Y., LI, S., SPELT, C., DI SANSEBASTIANO, G. P., REALE, L., FERRANTI, F., VERWEIJ, W., KOES, R. & QUATTROCCHIO, F. M. 2017. A Tonoplast P3B-ATPase Mediates Fusion of Two Types of Vacuoles in Petal Cells. Cell Rep, 19, 2413-2422.
Pubmed: Author and Title
Google Scholar: Author Only Title Only Author and Title

FASSHAUER, D., ELIASON, W. K., BRUNGER, A. T. & JAHN, R. 1998. Identification of a minimal core of the synaptic SNARE complex sufficient for reversible assembly and disassembly. Biochemistry, 37, 10354-10362.
Pubmed: Author and Title
Google Scholar: Author Only Title Only Author and Title

FENDRYCH, M., LEUNG, J. & FRIML, J. 2016. TIR1/AFB-Aux/IAA auxin perception mediates rapid cell wall acidification and growth of Arabidopsis hypocotyls. Elife, 5.
Pubmed: Author and Title
Google Scholar: Author Only Title Only Author and Title

FORESTI, O., DASILVA, L. L. P. & DENECKE, J. 2006. Overexpression of the Arabidopsis syntaxin PEP12/SYP21 inhibits transport from the prevacuolar compartment to the lytic vacuole in vivo. Plant Cell, 18, 2275-2293.
Pubmed: Author and Title
Google Scholar: Author Only Title Only Author and Title

FUGLSANG, A. T., BORCH, J., BYCH, K., JAHN, T. P., ROEPSTORFF, P. & PALMGREN, M. G. 2003. The binding site for regulatory 14-3-3 protein in plant plasma membrane H+-ATPase: involvement of a region promoting phosphorylation-independent interaction in addition to the phosphorylation-dependent C-terminal end. J Biol Chem, 278, 42266-72.
Pubmed: Author and Title
Google Scholar: Author Only Title Only Author and Title

FUJIWARA, M., UEMURA, T., EBINE, K., NISHIMORI, Y., UEDA, T., NAKANO, A., SATO, M. H. & FUKAO, Y. 2014. Interactomics of Qa-SNARE in Arabidopsis thaliana. Plant and Cell Physiology, 55, 781-789.
Pubmed: Author and Title
Google Scholar: Author Only Title Only Author and Title

GAFFIELD, M. A. & BETZ, W. J. 2006. Imaging synaptic vesicle exocytosis and endocytosis with FM dyes. Nat Protoc, 1, 2916-21.
Pubmed: Author and Title
Google Scholar: Author Only Title Only Author and Title

GEELEN, D., LEYMAN, B., BATOKO, H., DI SANSEBASTIANO, G. P., MOORE, I. & BLATT, M. R. 2002. The abscisic acid-related SNARE homolog NtSyr1 contributes to secretion and growth: evidence from competition with its cytosolic domain. Plant Cell, 14, 387-406.
Pubmed: Author and Title
Google Scholar: Author Only Title Only Author and Title

GELDNER, N., ANDERS, N., WOLTERS, H., KEICHER, J., KORNBERGER, W., MULLER, P., DELBARRE, A., UEDA, T., NAKANO, A. & JURGENS, G. 2003. The Arabidopsis GNOM ARF-GEF mediates endosomal recycling, auxin transport, and auxin-dependent plant growth. Cell, 112, 219-230.
Pubmed: Author and Title
Google Scholar: Author Only Title Only Author and Title

GREFEN, C. & BLATT, M. R. 2012. A 2in1 cloning system enables ratiometric bimolecular fluorescence complementation (rBiFC). Biotechniques, 53, 311-314.
Pubmed: Author and Title
Google Scholar: Author Only Title Only Author and Title

GREFEN, C., DONALD, N., HASHIMOTO, K., KUDLA, J., SCHUMACHER, K. & BLATT, M. R. 2010. A ubiquitin-10 promoter-based vector set for fluorescent protein tagging facilitates temporal stability and native protein distribution in transient and stable expression studies. Plant Journal, 64, 355-365.
Pubmed: Author and Title
Google Scholar: Author Only Title Only Author and Title

GREFEN, C., KARNIK, R., LARSON, E., LEFOULON, C., WANG, Y., WAGHMARE, S., ZHANG, B., HILLS, A. & BLATT, M. R. 2015. A vesicle-trafficking protein commandeers Kv channel voltage sensors for voltage-dependent secretion. Nat Plants, 1, 15108.
Pubmed: Author and Title
Google Scholar: Author Only Title Only Author and Title

HAGER, A. 2003. Role of the plasma membrane H+-ATPase in auxin-induced elongation growth: historical and new aspects. J Plant Res, 116, 483-505.
Pubmed: Author and Title
Google Scholar: Author Only Title Only Author and Title

HAGER, A., DEBUS, G., EDEL, H. G., STRANSKY, H. & SERRANO, R. 1991. Auxin induces exocytosis and the rapid synthesis of a high-turnover pool of plasma-membrane H(+)-ATPase. Planta, 185, 527-37.
Pubmed: Author and Title
Google Scholar: Author Only Title Only Author and Title

HAGER, A., MENZEL, H. & KRAUSS, A. 1971. [Experiments and hypothesis concerning the primary action of auxin in elongation growth]. Planta, 100, 47-75.
Pubmed: Author and Title
Google Scholar: Author Only Title Only Author and Title

HARPER, J. F., SUROWY, T. K. & SUSSMAN, M. R. 1989. Molecular cloning and sequence of cDNA encoding the plasma membrane proton pump (H + -ATPase) of Arabidopsis thaliana Proceedings Of The National Academy Of Sciences Of The United States Of America, 86, 1234-1238.
Pubmed: Author and Title
Google Scholar: Author Only Title Only Author and Title

HARRISON, S. J., MOTT, E. K., PARSLEY, K., ASPINALL, S., GRAY, J. C. & COTTAGE, A. 2006. A rapid and robust method of identifying transformed Arabidopsis thaliana seedlings following floral dip transformation. Plant Methods, 2, 19.
Pubmed: Author and Title
Google Scholar: Author Only Title Only Author and Title

HARUTA, M., BURCH, H. L., NELSON, R. B., BARRETT-WILT, G., KLINE, K. G., MOHSIN, S. B., YOUNG, J. C., OTEGUI, M. S. & SUSSMAN, M. R. 2010. Molecular characterization of mutant Arabidopsis plants with reduced plasma membrane proton pump activity. J Biol Chem, 285, 17918-29.
Pubmed: Author and Title
Google Scholar: Author Only Title Only Author and Title

HARUTA, M., GRAY, W. M. & SUSSMAN, M. R. 2015. Regulation of the plasma membrane proton pump (H+-ATPase) by phosphorylation. Current Opinion in Plant Biology, 28, 68-75.
Pubmed: Author and Title
Google Scholar: Author Only Title Only Author and Title

HARUTA, M. & SUSSMAN, M. R. 2012. The effect of a genetically reduced plasma membrane protonmotive force on vegetative growth of Arabidopsis thaliana Plant Physiology, doi:10.1104/pp.111.189167.
Pubmed: Author and Title
Google Scholar: Author Only Title Only Author and Title

HASHIMOTO-SUGIMOTO, M., HIGAKI, T., YAENO, T., NAGAMI, A., IRIE, M., FUJIMI, M., MIYAMOTO, M., AKITA, K., NEGI, J., SHIRASU, K., HASEZAWA, S. & IBA, K. 2013. A Munc13-like protein in Arabidopsis mediates H+-ATPase translocation that is essential for stomatal responses. Nature Communications, 4.
Pubmed: Author and Title
Google Scholar: Author Only Title Only Author and Title

HEARD, W., SKLENÁŘ, J., TOMÉ, D. F. A., ROBATZEK, S. & JONES, A. M. E. 2015. Identification of Regulatory and Cargo Proteins of Endosomal and Secretory Pathways in Arabidopsis thaliana by Proteomic Dissection. Molecular & Cellular Proteomics : MCP, 14, 1796-1813.
Pubmed: Author and Title
Google Scholar: Author Only Title Only Author and Title

HECKER, A., WALLMEROTH, N, PETER, S, BLATT, MR, HARTER, K, GREFEN, C 2015. Binary 2in1 vectors improve in planta (co-) localisation and dynamic protein interaction studies. Plant Physiology, 168, 776-87.
Pubmed: Author and Title
Google Scholar: Author Only Title Only Author and Title

HIGAKI, T., HASHIMOTO-SUGIMOTO, M., AKITA, K., IBA, K. & HASEZAWA, S. 2014. Dynamics and environmental responses of PATROL1 in Arabidopsis subsidiary cells. Plant Cell Physiol, 55, 773-80.
Pubmed: Author and Title

Google Scholar: Author Only Title Only Author and Title

HONSBEIN, A., SOKOLOVSKI, S., GREFEN, C., CAMPANONI, P., PRATELLI, R., PANEQUE, M., CHEN, Z., JOHANSSON, I. & BLATT, M. R. 2009. A tripartite SNARE-K+ channel complex mediates in channel-dependent K+ nutrition in Arabidopsis. Plant Cell, 21, 2859-77.
Pubmed: Author and Title
Google Scholar: Author Only Title Only Author and Title

HUISMAN, R., HONTELEZ, J., MYSORE, K. S., WEN, J., BISSELING, T. & LIMPENS, E. 2016. A symbiosis-dedicated SYNTAXIN OF PLANTS 13II isoform controls the formation of a stable host-microbe interface in symbiosis. New Phytol, 211, 1338-51.
Pubmed: Author and Title
Google Scholar: Author Only Title Only Author and Title

ICHIKAWA, M., HIRANO, T., ENAMI, K., FUSELIER, T., KATO, N., KWON, C., VOIGT, B., SCHULZE-LEFERT, P., BALUSKA, F. & SATO, M. H. 2014. Syntaxin of plant proteins SYP123 and SYP132 mediate root hair tip growth in Arabidopsis thaliana. Plant Cell Physiol, 55, 790-800.
Pubmed: Author and Title
Google Scholar: Author Only Title Only Author and Title

JAHN, R. & SCHELLER, R. H. 2006. SNAREs - engines for membrane fusion. Nature Reviews Molecular Cell Biology, 7, 631-643.
Pubmed: Author and Title
Google Scholar: Author Only Title Only Author and Title

JEZEK, M. & BLATT, M. R. 2017. The Membrane Transport System of the Guard Cell and Its Integration for Stomatal Dynamics. Plant Physiol, 174, 487-519.
Pubmed: Author and Title
Google Scholar: Author Only Title Only Author and Title

KALDE, M., NUHSE, T. S., FINDLAY, K. & PECK, S. C. 2007. The syntaxin SYP132 contributes to plant resistance against bacteria and secretion of pathogenesis-related protein 1. Proceedings Of The National Academy Of Sciences Of The United States Of America, 104, 11850-11855.
Pubmed: Author and Title
Google Scholar: Author Only Title Only Author and Title

KARGUL, J., GANSEL, X., TYRRELL, M., STICHER, L. & BLATT, M. R. 2001. Protein-binding partners of the tobacco syntaxin NtSyr1. FEBS Letters, 508, 253-258.
Pubmed: Author and Title
Google Scholar: Author Only Title Only Author and Title

KARIMI, M., INZE, D. & DEPICKER, A. 2002. GATEWAY vectors for Agrobacterium -mediated plant transformation. Trends In Plant Science, 7, 193-195.
Pubmed: Author and Title
Google Scholar: Author Only Title Only Author and Title

KARNAHL, M., PARK, M., KRAUSE, C., HILLER, U., MAYER, U., STIERHOF, Y. D. & JURGENS, G. 2018. Functional diversification of Arabidopsis SEC1-related SM proteins in cytokinetic and secretory membrane fusion. Proc Natl Acad Sci U S A, 115, 6309-6314.
Pubmed: Author and Title
Google Scholar: Author Only Title Only Author and Title

KARNIK, R., GREFEN, C., BAYNE, R., HONSBEIN, A., KOHLER, T., KIOUMOURTZOGLOU, D., WILLIAMS, M., BRYANT, N. J. & BLATT, M. R. 2013. Arabidopsis Sec1/Munc18 protein SEC11 is a competitive and dynamic modulator of SNARE binding and SYP121-dependent vesicle traffic. Plant Cell, 25, 1368-82.
Pubmed: Author and Title
Google Scholar: Author Only Title Only Author and Title

KARNIK, R., WAGHMARE, S., ZHANG, B., LARSON, E., LEFOULON, C., GONZALEZ, W. & BLATT, M. R. 2017. Commandeering Channel Voltage Sensors for Secretion, Cell Turgor, and Volume Control. Trends Plant Sci, 22, 81-95.
Pubmed: Author and Title
Google Scholar: Author Only Title Only Author and Title

KARNIK, R., ZHANG, B., WAGHMARE, S., ADERHOLD, C., GREFEN, C. & BLATT, M. R. 2015. Binding of SEC11 indicates its role in SNARE recycling after vesicle fusion and identifies two pathways for vesicular traffic to the plasma membrane. Plant Cell, 27, 675-94.
Pubmed: Author and Title
Google Scholar: Author Only Title Only Author and Title

KAUNDAL, A., RAMU, V. S., OH, S., LEE, S., PANT, B., LEE, H. K., ROJAS, C. M., SENTHIL-KUMAR, M. & MYSORE, K. S. 2017. GENERAL CONTROL NONREPRESSIBLE4 Degrades 14-3-3 and the RIN4 Complex to Regulate Stomatal Aperture with Implications on Nonhost Disease Resistance and Drought Tolerance. Plant Cell, 29, 2233-2248.
Pubmed: Author and Title
Google Scholar: Author Only Title Only Author and Title

KINOSHITA, T. & SHIMAZAKI, K. 1999. Blue light activates the plasma membrane H+ -ATPase by phosphorylation of the C-terminus in stomatal guard cells. EMBO Journal, 18, 5548-5558.
Pubmed: Author and Title
Google Scholar: Author Only Title Only Author and Title

KITAKURA, S., VANNESTE, S., ROBERT, S., LOFKE, C., TEICHMANN, T., TANAKA, H. & FRIML, J. 2011. Clathrin mediates endocytosis and polar distribution of PIN auxin transporters in Arabidopsis. Plant Cell, 23, 1920-31.
Pubmed: Author and Title
Google Scholar: Author Only Title Only Author and Title

LARSON, E. R., VAN ZELM, E., ROUX, C., MARION-POLL, A. & BLATT, M. R. 2017. Clathrin Heavy Chain Subunits Coordinate Endo- and Exocytic Traffic and Affect Stomatal Movement. Plant Physiol, 175, 708-720.
Pubmed: Author and Title
Google Scholar: Author Only Title Only Author and Title

LEE, M. H., MIN, M. K., LEE, Y. J., JIN, J. B., SHIN, D. H., KIM, D. H., LEE, K. H. & HWANG, I. 2002. ADP-ribosylation factor 1 of Arabidopsis plays a critical role in intracellular trafficking and maintenance of endoplasmic reticulum morphology in Arabidopsis. Plant Physiol, 129, 1507-20.
Pubmed: Author and Title
Google Scholar: Author Only Title Only Author and Title

LIMPENS, E., IVANOV, S., VAN ESSE, W., VOETS, G., FEDOROVA, E. & BISSELING, T. 2009. Medicago N2-fixing symbiosomes acquire the endocytic identity marker Rab7 but delay the acquisition of vacuolar identity. Plant Cell, 21, 2811-28.
Pubmed: Author and Title
Google Scholar: Author Only Title Only Author and Title

LIVAK, K. J. & SCHMITTGEN, T. D. 2001. Analysis of relative gene expression data using real-time quantitative PCR and the 2(-Delta Delta C(T)) Method. Methods, 25, 402-8.
Pubmed: Author and Title
Google Scholar: Author Only Title Only Author and Title

MACROBBIE, E. A. C. 1991. Effect of ABA on ion transport and stomatal regulation. In: DAVIES, W. J. & JONES, H. G. (eds.) Abscisic Acid Physiology and Biochemistry. Oxford: Bios Scientific.
Pubmed: Author and Title
Google Scholar: Author Only Title Only Author and Title

MARRE, E. 1979. FUSICOCCIN - TOOL IN PLANT PHYSIOLOGY. Annual Review of Plant Physiology and Plant Molecular Biology, 30, 273-288.
Pubmed: Author and Title
Google Scholar: Author Only Title Only Author and Title

MARWAHA, R. & SHARMA, M. 2017. DQ-Red BSA Trafficking Assay in Cultured Cells to Assess Cargo Delivery to Lysosomes. Bio Protoc, 7.
Pubmed: Author and Title
Google Scholar: Author Only Title Only Author and Title

MECKEL, T., HURST, A. C., THIEL, G. & HOMANN, U. 2004. Endocytosis against high turgor: intact guard cells of Vicia faba constitutively endocytose fluorescently labelled plasma membrane and GFP-tagged K-channel KAT1. Plant J, 39, 182-93.
Pubmed: Author and Title
Google Scholar: Author Only Title Only Author and Title

MERLOT, S., LEONHARDT, N., FENZI, F., VALON, C., COSTA, M., PIETTE, L., VAVASSEUR, A., GENTY, B., BOIVIN, K., MULLER, A., GIRAUDAT, J. & LEUNG, J. 2007. Constitutive activation of a plasma membrane H(+)-ATPase prevents abscisic acid-mediated stomatal closure. EMBO J, 26, 3216-26.
Pubmed: Author and Title
Google Scholar: Author Only Title Only Author and Title

MICHELET, B. & BOUTRY, M. 1995. The Plasma Membrane H+-ATPase (A Highly Regulated Enzyme with Multiple Physiological Functions). Plant Physiol, 108, 1-6.
Pubmed: Author and Title
Google Scholar: Author Only Title Only Author and Title

OMELYANCHUK, N. A., WIEBE, D. S., NOVIKOVA, D. D., LEVITSKY, V. G., KLIMOVA, N., GORELOVA, V., WEINHOLDT, C., VASILIEV, G. V., ZEMLYANSKAYA, E. V., KOLCHANOV, N. A., KOCHETOV, A. V., GROSSE, I. & MIRONOVA, V. V. 2017. Auxin regulates functional gene groups in a fold-change-specific manner in Arabidopsis thaliana roots. Sci Rep, 7, 2489.
Pubmed: Author and Title
Google Scholar: Author Only Title Only Author and Title

PALMGREN, M. G. 2001. Plant plasma membrane H+ -ATPases: Powerhouses for nutrient uptake. Annual Review Of Plant Physiology And Plant Molecular Biology, 52, 817-845.
Pubmed: Author and Title
Google Scholar: Author Only Title Only Author and Title

PALMGREN, M. G., BAEKGAARD, L., LOPEZ-MARQUES, R. L. & FUGLSANG, A. T. 2011. Plasma Membrane ATPases. In: MURPHY, A., PEER, W. A. & SCHULZ, B. (eds.) Plant Plasma Membrane.
Pubmed: Author and Title
Google Scholar: Author Only Title Only Author and Title

PAN, H., OZTAS, O., ZHANG, X., WU, X., STONOHA, C., WANG, E., WANG, B. & WANG, D. 2016. A symbiotic SNARE protein generated by

alternative termination of transcription. Nat Plants, 2, 15197.
Pubmed: Author and Title
Google Scholar: Author Only Title Only Author and Title

PARK, M., KRAUSE, C., KARNAHL, M., REICHARDT, I., EL KASMI, F., MAYER, U., STIERHOF, Y. D., HILLER, U., STROMPEN, G., BAYER, M., KIENTZ, M., SATO, M. H., NISHIMURA, M. T., DANGL, J. L., SANDERFOOT, A. A. & JURGENS, G. 2018. Concerted Action of Evolutionarily Ancient and Novel SNARE Complexes in Flowering-Plant Cytokinesis. Dev Cell, 44, 500-511 e4.
Pubmed: Author and Title
Google Scholar: Author Only Title Only Author and Title

RAFIQI, M., GAN, P. H. P., RAVENSDALE, M., LAWRENCE, G. J., ELLIS, J. G., JONES, D. A., HARDHAM, A. R. & DODDS, P. N. 2010. Internalization of Flax Rust Avirulence Proteins into Flax and Tobacco Cells Can Occur in the Absence of the Pathogen. Plant Cell, 22, 2017-2032.
Pubmed: Author and Title
Google Scholar: Author Only Title Only Author and Title

RAYLE, D. L. & CLELAND, R. 1970. Enhancement of wall loosening and elongation by Acid solutions. Plant Physiol, 46, 250-3.
Pubmed: Author and Title
Google Scholar: Author Only Title Only Author and Title

ROELFSEMA, M. R. G. & HEDRICH, R. 2005. In the light of stomatal opening: new insights into 'the Watergate'. New Phytologist, 167, 665-691.
Pubmed: Author and Title
Google Scholar: Author Only Title Only Author and Title

SANDERFOOT, A. 2007. Increases in the number of SNARE genes parallels the rise of multicellularity among the green plants. Plant Physiology, 144, 6-17.
Pubmed: Author and Title
Google Scholar: Author Only Title Only Author and Title

SAPONARO, A., PORRO, A., CHAVES-SANJUAN, A., NARDINI, M., RAUH, O., THIEL, G. & MORONI, A. 2017. Fusicoccin Activates KAT1 Channels by Stabilizing Their Interaction with 14-3-3 Proteins. Plant Cell, 29, 2570-2580.
Pubmed: Author and Title
Google Scholar: Author Only Title Only Author and Title

SCHINDELIN, J., ARGANDA-CARRERAS, I., FRISE, E., KAYNIG, V., LONGAIR, M., PIETZSCH, T., PREIBISCH, S., RUEDEN, C., SAALFELD, S., SCHMID, B., TINEVEZ, J.-Y., WHITE, D. J., HARTENSTEIN, V., ELICEIRI, K., TOMANCAK, P. & CARDONA, A. 2012. Fiji: an open-source platform for biological-image analysis. Nature Methods, 9, 676.
Pubmed: Author and Title
Google Scholar: Author Only Title Only Author and Title

SCHINDLER, T., BERGFELD, R., HOHL, M. & SCHOPFER, P. 1994. Inhibition of golgi apparatus function by brefeldin A in maize coleoptiles and its consequences on auxin-mediated growth, cell- wall extensibility and secretion of cell wall proteins. Planta, 192, 404-413.
Pubmed: Author and Title
Google Scholar: Author Only Title Only Author and Title

SHIMAZAKI, K. I., DOI, M., ASSMANN, S. M. & KINOSHITA, T. 2007. Light regulation of stomatal movement. Annual Review of Plant Biology, 58, 219-247.
Pubmed: Author and Title
Google Scholar: Author Only Title Only Author and Title

SHOPE, J. C., PEAK, D. & MOTT, K. A. 2008. Stomatal responses to humidity in isolated epidermes. Plant Cell And Environment, 31, 1290-1298.
Pubmed: Author and Title
Google Scholar: Author Only Title Only Author and Title

SKLODOWSKI, K., RIEDELSBERGER, J., RADDATZ, N., RIADI, G., CABALLERO, J., CHEREL, I., SCHULZE, W., GRAF, A. & DREYER, I. 2017. The receptor-like pseudokinase MRH1 interacts with the voltage-gated potassium channel AKT2. Sci Rep, 7, 44611.
Pubmed: Author and Title
Google Scholar: Author Only Title Only Author and Title

SONDERGAARD, T. E., SCHULZ, A. & PALMGREN, M. G. 2004. Energization of transport processes in plants. roles of the plasma membrane H+-ATPase. Plant Physiol, 136, 2475-82.
Pubmed: Author and Title
Google Scholar: Author Only Title Only Author and Title

SUDHOF, T. C. & ROTHMAN, J. E. 2009. Membrane Fusion: Grappling with SNARE and SM Proteins. Science, 323, 474-477.
Pubmed: Author and Title
Google Scholar: Author Only Title Only Author and Title

SUTTER, J. U., CAMPANONI, P., TYRRELL, M. & BLATT, M. R. 2006. Selective mobility and sensitivity to SNAREs is exhibited by the Arabidopsis KAT1 K+ channel at the plasma membrane. Plant Cell, 18, 935-954.
Pubmed: Author and Title
Google Scholar: Author Only Title Only Author and Title

SUTTER, J. U., SIEBEN, C., HARTEL, A., EISENACH, C., THIEL, G. & BLATT, M. R. 2007. Abscisic acid triggers the endocytosis of the Arabidopsis KAT1 K+ channel and its recycling to the plasma membrane. Current Biology, 17, 1396-1402.
Pubmed: Author and Title
Google Scholar: Author Only Title Only Author and Title

SZE, H., LI, X. H. & PALMGREN, M. G. 1999. Energization of plant cell membranes by H+ -pumping ATPases: Regulation and biosynthesis. Plant Cell, 11, 677-689.
Pubmed: Author and Title
Google Scholar: Author Only Title Only Author and Title

THIEL, G., BLATT, M. R., FRICKER, M. D., WHITE, I. R. & MILLNER, P. 1993. Modulation of K+ channels in Vicia stomatal guard cells by peptide homologs to the auxin-binding protein C terminus. Proc Natl Acad Sci U S A, 90, 11493-7.
Pubmed: Author and Title
Google Scholar: Author Only Title Only Author and Title

TYRRELL, M., CAMPANONI, P., SUTTER, J. U., PRATELLI, R., PANEQUE, M., SOKOLOVSKI, S. & BLATT, M. R. 2007. Selective targeting of plasma membrane and tonoplast traffic by inhibitory (dominant-negative) SNARE fragments. Plant J, 51, 1099-115.
Pubmed: Author and Title
Google Scholar: Author Only Title Only Author and Title

VELASQUEZ, S. M., BARBEZ, E., KLEINE-VEHN, J. & ESTEVEZ, J. M. 2016. Auxin and Cellular Elongation. Plant Physiology, 170, 1206-1215.
Pubmed: Author and Title
Google Scholar: Author Only Title Only Author and Title

VIALET-CHABRAND, S., HILLS, A., WANG, Y., GRIFFITHS, H., LEW, V. L., LAWSON, T., BLATT, M. R. & ROGERS, S. 2017. Global Sensitivity Analysis of OnGuard Models Identifies Key Hubs for Transport Interaction in Stomatal Dynamics. Plant Physiol, 174, 680-688.
Pubmed: Author and Title
Google Scholar: Author Only Title Only Author and Title

WAGHMARE, S., LILEIKYTE, E., KARNIK, R., GOODMAN, J. K., BLATT, M. R. & JONES, A. M. E. 2018. SNAREs SYP121 and SYP122 Mediate the Secretion of Distinct Cargo Subsets. Plant Physiol, 178, 1679-1688.
Pubmed: Author and Title
Google Scholar: Author Only Title Only Author and Title

WANG, Y., NOGUCHI, K., ONO, N., INOUE, S. I., TERASHIMA, I. & KINOSHITA, T. 2014. Overexpression of plasma membrane H+ -ATPase in guard cells promotes light-induced stomatal opening and enhances plant growth. Proc.Nat.Acad.Sci.USA, 111, 533-538.
Pubmed: Author and Title
Google Scholar: Author Only Title Only Author and Title

XUE, Y., YANG, Y., YANG, Z., WANG, X. & GUO, Y. 2018. VAMP711 Is Required for Abscisic Acid-Mediated Inhibition of Plasma Membrane H(+)-ATPase Activity. Plant Physiol, 178, 1332-1343.
Pubmed: Author and Title
Google Scholar: Author Only Title Only Author and Title

YAMAUCHI, S., TAKEMIYA, A., SAKAMOTO, T., KURATA, T., TSUTSUMI, T., KINOSHITA, T. & SHIMAZAKI, K.-I. 2016. The Plasma Membrane H+-ATPase AHA1 Plays a Major Role in Stomatal Opening in Response to Blue Light. Plant Physiology, 171, 2731-2743.
Pubmed: Author and Title
Google Scholar: Author Only Title Only Author and Title

YANG, H. & MURPHY, A. 2013. Membrane Preparation, Sucrose Density Gradients and Two-phase Separation Fractionation from Five-day-old Arabidopsis seedlings. The Plant Journal.
Pubmed: Author and Title
Google Scholar: Author Only Title Only Author and Title

YOSHIDA, S., UEMURA, M., NIKI, T., SAKAI, A. & GUSTA, L. V. 1983. Partition of membrane particles in aqueous two-polymer phase system and its practical use for purification of plasma membranes from plants. Plant Physiol, 72, 105-14.
Pubmed: Author and Title
Google Scholar: Author Only Title Only Author and Title

ZHANG, B., KARNIK, R., DONALD, N. & BLATT, M. R. 2018. A GPI Signal Peptide-Anchored Split-Ubiquitin (GPS) System for Detecting Soluble Bait Protein Interactions at the Membrane. Plant Physiol, 178, 13-17.
Pubmed: Author and Title
Google Scholar: Author Only Title Only Author and Title

ZHANG, B., KARNIK, R., WANG, Y., WALLMEROTH, N., BLATT, M. R. & GREFEN, C. 2015. The Arabidopsis R-SNARE VAMP721 Interacts with KAT1 and KC1 K+ Channels to Moderate K+ Current at the Plasma Membrane. Plant Cell, 27, 1697-717.
Pubmed: Author and Title
Google Scholar: Author Only Title Only Author and Title

ZHANG, X., WANG, H. B., TAKEMIYA, A., SONG, C. P., KINOSHITA, T. & SHIMAZAKI, K. I. 2004. Inhibition of blue light-dependent H+ pumping by abscisic acid through hydrogen peroxide-induced dephosphorylation of the plasma membrane H+ -ATPase in guard cell protoplasts. Plant Physiology, 136, 4150-4158.